國立交通大學

機械工程學系

碩士論文

以微機電製程製作微型 PDMS 質子交換膜燃料電池之實驗研究

The Experimental Study on Micro PDMS PEMFC by Using MEMS Technology

研 究 生：許義嘉

指導教授：陳俊勳　教授

中華民國九十九年六月

以微機電製程製作微型 PDMS 質子交換膜燃料電池之實驗研究

The Experimental Study on Micro PDMS PEMFC Manufactured by Using MEMS Technology

研究生：許義嘉　　Student：Chih-Wei Cheng

指導教授：陳俊勳　　Advisor：Chiun-Hsun Chen

國 立 交 通 大 學

機 械 工 程 學 系

碩 士 論 文

A Thesis

Submitted to Department of Mechanical Engineering

College of Engineering

National Chiao Tung University

In Partial Fulfiillment of the Requirements

For the Degree of

Master of Science

In Mechanical Engineering

June 2010

Hsinchu, Taiwan, Republic of China

中 華 民 國 九 十 九 年 六 月

The Experimental Study on Micro PDMS PEMFC Manufactured by Using MEMS Technology

以微機電製程製作微型 PDMS 質子交換膜燃料電池之實驗研究

學 生:許 義 嘉　　指導教授:陳俊勳

國立交通大學機械工程學系

摘要

本文主要為研究以微機電製程製作微型 PDMS 質子交換膜燃料電池之實驗測試。探討反應面積為 2 公分x2 公分的單電池。第一部分是 PDMS(聚二甲基矽氧烷)單電池之研究，實驗參數包括集電片開孔形狀、對流方式、以及組裝時鎖合扭力的影響；第二部分是 PDMS 平板電池堆的研究，實驗參數包括鎖合扭力以及燃料供應方式的影響；另外，單電池及電池堆都經由長時間放電測試以觀察其耐久度。最後，本論文也將 PDMS 微型燃料電池與矽微型燃料電池做性能的比較與分析。

由實驗結果可知在相同開孔率之集電片下，不論陰極採用呼吸式或是強制對流式 (有流場板)之單電池，其性能皆隨集電片之開孔數增加而提升；強制對流方式的單電池比較適合高電流密度輸出使用，而呼吸式燃料電池較適合低電流長時間輸出使用；電池組裝之鎖合壓力必須在不使流道結構變型的情況下增加才能有效提升其性能；對於本實驗之電池堆設計，由於陰極端的空氣提供速率有限，因此增加燃料流量並無法有效改善濃度極化現象；另外，電池堆中之每顆單電池因為燃料供應順序不同而會有不同性能表現；單電池與電池堆經過十四小時長時間測試後，都有良好的耐久度；經比較後，不論陰極採用呼吸式或是強制對流式，PDMS 基材之單電池皆比矽基材之單電池性能表現佳；由於 PDMS 基材有比較少的積水現象，因此比矽基材更適合用在呼吸式微型燃料電池上。

關鍵字：微機電，PDMS，微型質子交換膜燃料電池，開孔率，鎖合壓力

The Experimental Study on Micro PDMS PEMFC Manufactured by Using MEMS Technology

Student: Yi-Ja Hsu Advisor: Prof. Chiun-Hsun Chen

Department of Mechanical Engineering
National Chiao Tung University

ABSTRACT

This study fabricated micro PDMS (Polydimethyl Siloxane) PEMFC (Proton Exchange Membrane Fuel Cell) by using the MEMS (Micro Electro Mechanical Systems) technology. The active area of the membrane is 2cm×2cm. Firstly, a series of performance experiments on a single micro PDMS PEMFC was carried out. The experimental parameters included current collector shape, convection type and clamping force, respectively. Secondly, a planar PEMFC stack was designed and assembled to test the performance. The experimental parameters consisted of clamping force and fuel supply condition. In addition, both the single cell and the stack were tested for durability. Finally, a comparison between PDMS-based PEMFC and silicon-based one was made.

The experimental results show that both the performances of the air-breathing and forced convection cells increase with an increase of the circle numbers from one to twenty-five on the current collector under the same current collector open ratio; The forced convection cell is a better choice for long-time high current-density output whereas the air-breathing cell is more suitable for lower current density output; An appropriate clamping torque should be considered carefully to enhance the performance but without narrowing down the fuel flow channels; The increase of flow rate is not a best way to improve the concentration loss in this air-breathing stack experiment because of the limiting air supply, and each cell in the same stack has different performance under series arrangement; Both the single micro PDMS fuel cell and the cell stack can maintain a stable power output for a long time use up to 14 hours; The PDMS-based PEMFC has a better performance than that of the silicon-based one under both forced oxygen supply and the air-breathing ways; PDMS is a better material than silicon for micro air-breathing fuel

cell because it is with less water flooding effects.

Keywords: MEMS, PDMS, Micro PEMFC, Open Ratio, Clamping Force

Acknowledgements

曾經徬徨，曾經失望，曾經面對未知的挑戰排回躊躇，曾經跌於險阻的路途灰心喪志。但很幸運的，我－許義嘉，一個呆呆蠢蠢的平凡學生，也終於完成了碩士學位。這期間得到了好多人幫助，我才能克服挫折而成長。謝謝你們的相伴，要感謝的人太多了，所以就感謝天吧……開玩笑的，我還是要一一點名出來。

感謝我的指導教授　陳俊勳，除了論文的指導外，您不時耳提面命要我對自己負責，相信我能做得更好，我想這才是兩年中獲得的最大的淬煉。感謝阿貴學長在燃料電池研究上不厭其煩的教導，因為你不疾不徐的從容態度，才使我因挫折而沮喪擔憂的心情得到舒緩。致瑋學長的開路減少我的絆倒機會，長新立下的好榜樣讓我有努力目標，也感謝堂原學長在實驗上的協助。感謝金輝學長，你常主動提供研究上與生活上的建議，使我的研究之路更順遂。感謝云婷與聖容學妹，妳們讓我感受笑聲與溫暖，也讓我分享生活的快樂悲傷，更讓我有依依不捨的心情。感謝信錡、瑋琮，你們讓我感到並肩作戰、同甘共苦的溫馨，這場仗打得並不寂寞。感謝實驗室其他成員:彥成、達叔、家維學長，嘉軒、世庸、宗翰、黃鈞，你們都是我實驗室生活的愉快回憶。

感謝郭勅君、大玉米和姿妤，失落的時候有你們在，抱怨的時

候有你們在，炫耀的時候有你們在，與你們一起渡過的日子，讓我的學生生涯好精彩。感謝濃眉團：小傑、當肯、豪瓜、毛毛、堯琦，在同儕們相繼分道揚鑣之際，你們的陪伴讓我在吉他社得到溫馨感，也感謝吉他社歷屆成員們這六年的陪伴。感謝小玄子，我重要的同鄉和玩伴。感謝也許星期三，和小馬、BB 你們一起表演，生活變得很充實，也讓我重新思考浪漫、夢想的重要性。

感謝我的父母親，雖然這六年來總是因為相聚遙遠，無法常常回家，但愛你們的心一直不會變。感謝妹妹，不論生病還瑣事，妳的照顧是我的避風港。感謝奶奶一家人，你們總以我為榮，給予我精神支持。感謝台北的華姑，讓我假日有回家的感覺。

我沒提到的朋友，你們都是我生命中重要的過客，成就了這本論文，也成就了我目前為止小小的人生，感謝你們。

對於前途、對於夢想，總在不斷探索中前進，就算現在無法得到答案，至少得到了一份能力與一股信念：實現夢想的能力，相信自己的信念。碩士學位並不值得說嘴，但這期間擁有的回憶，卻足以讓我炫耀一輩子。

P.S. 也感謝我的娛樂夥伴：Friends 影集、吉他，排遣我心煩意亂的煩躁時光。

Contents

LIST OF TABLE

LIST OF FIGURES

Chapter 1

Introduction

1.1 Motivation and Background:

Facing the problems that the combustion of fossil fuels releases harmful emissions into the air as shown in Fig. 1.1 that can cause the Greenhouse Effect and threat the health of human beings, the need of clean, no-pollution energy becomes more and more eager. These emissions, such as CO_2, CH_4, and N_2O, etc. not only can penetrate deep into the lungs and remain there for months or even years, but also can cause severe damage to environment like the acid rain and global warming. Besides, the price of petroleum has been soared due to its rapid depletion in recent years (Fig. 1.2), as a consequence, looking for the alternative energy resources now is a crucial issue for mankind.

In fact, there are several ways by which the emissions by human activities can be curbed, and the dependence on fossil fuels can be reduced without diminishing the living standard. In addition to improving the efficiencies of end-use equipments, vehicle propulsion engines as well as power generation facilities, the increasing applications of renewable or alternative energy sources, such as wind, sun, water, nuclear, bio and hydrogen, should also be take into consideration. Fuel cells, offering the advantage of no or negligible emission of gaseous products, have been expected to be one of the green energy sources in 21st century.

Not only without emission, fuel cells also have some other advantages: high electrochemical performance efficiency, simple stacks design, noise-free, no moving part and low temperature operation, and

these characteristics make fuel cells a quite promising energy technology attractive for a variety of applications in recent years. The efficiency is one of the most distinguishing features for fuel cells. Unlike internal combustion engine, fuel cells are not subject to the limit of Carnot efficiency. Indeed, it's commonly supposed that if there were no "irreversibilities" then the efficiency could be 100%.

The proton exchange membrane fuel cell (PEMFC), or PEM fuel cell, is the most common-used one among all types of fuel cells due to its relatively low operation temperature. It can serve as a power source from a few watts for powering mobile phones and other electronic equipments, such as personal computer and notebook, right through to several kilowatts for boats and domestic systems, and to tens of kilowatts for cars, to hundreds of kilowatts for buses and industrial Combined Heat and Power (CHP) systems; see Fig. 1.3.

According to fuel type, PEMFC can be divided into two major categories, the hydrogen and the methanol. Comparing methanol with hydrogen, the former has two sever problems, which are slow fuel anode reactions process and fuel crossover (mixed potential), that make its performance lower than the latter one. Moreover, methanol is harmful to human, and its production of CO can poison Pt catalyst. In addition, methanol PEMFC can produce CO_2 whereas the product of hydrogen-oxygen PEMFC is the water only. Therefore, the application of hydrogen fuel in PEMFC is more preferred.

The basic operation of the hydrogen-oxygen fuel cell is very simple. Gaseous hydrogen and oxygen are supplied to anode and cathode, respectively. At the anode, hydrogen gas is catalyzed by Pt and ionizes,

releasing electrons and creating hydrogen ion H+, while at the cathode oxygen reacts with electrons coming from the electrode to form water. Followings are the individual and overall reactions:

$$\text{Anode: } H_2 \xrightarrow{Pt} 2H^+ + 2e^- \quad (1\text{-}1)$$

$$\text{Cathode: } \frac{1}{2}O_2 + 2H^+ + 2e^- \rightarrow H_2O + Heat \quad (1\text{-}2)$$

$$\text{Overall: } H_2 + \frac{1}{2}O_2 \rightarrow H_2O + Heat \quad (1\text{-}3)$$

The conventional fuel cells are in the order of Kilowatt, which is too large for 3C commercial products. Therefore, there are many researches recently to develop micro fuel cells that can be used as a portable power source to meet the power demands of a variety of 3C applications.

The previous efforts were mainly focused on the development of miniature PEMFC. In order to achieve this goal, Cheng [1] intended to make an effort in fabricating the micro fuel cell on silicon-based wafer by using the technology Micro Electro Mechanical System (MEMS) and to see its feasibility. His work found that the material of current collector slices have great influence on the performance of micro PEMFC, and the larger open ratio can obviously promote the micro PEMFC performance.

However, the structure of silicon-based flow field plate is too weak to prevent the problem of crack while assembling, and its nonelastic property easily causes the gas-leaking problem. Therefore, it is necessary to find a better way or better material to replace the silicon-based one, and retain the performance. A new material, Polydimethyl Siloxane (PDMS; $(H_3C)_3SiO[Si(CH_3)_2O]nSi(CH_3)_3$), is proposed in this work. It is a group of polymeric organosilicon compounds, whose properties are similar to those of silicones. Owing to its good biocompatibility and flow

property, the application of PDMS ranges from contact lenses and medical devices to flow delivery in microfluidic chips, elastic stamp, etc. In this study, it will take the advantage of its good plasticity, elasticity and molding quality to replace the silicon-based flow field plate [1].

1.2 Literature Review:

The flow field structures in fuel cells have to meet several requirements, such as homogeneous fluid distribution, product water removal, good current transport, good under-rib convection and high conductivity. Each factor can considerably influence the performance of fuel cells. However, this work, as mentioned previously, is focused on the effects of flow field structure, cell conductivity and stack assembly on the performance of micro PEMFC.

Yu et al. [2] successfully fabricated a miniature fuel cell on silicon wafers using micro-electronic fabrication techniques, which included photolithography, dry and wet etching, chemical and physical vapor deposition. They found that sputtering different thicknesses of Cu/Au (including 0.5μmAu, 0.2μm Au plated 1.4μm Cu, and 0.9μm Au plated 1.5μm Cu) composite layer on the top of the silicon wafer as a current collector can reduce the resistance, indicating that the cell performance is improved by increasing the thickness of the composite layer on the silicon wafer.

Meyers and Maynard [3] used MEMS techniques to fabricate micro flow channels of PEM fuel cell on silicon substrate. Their designs consisted of bipolar design, similar to the standard cell sandwich commonly used in PEMFC system, and monolithic design, essentially an

“unfolded” fuel cell with the anode and cathode on the same substrate (see Fig. 1.4). By making comparison, they found the former shows a better performance than the latter as illustrated in Fig. 1-5. The research also suggested that many system-level issues, like thermal management, air movement, fuel delivery, humidification control, water management, power load management and system integration, must be considered in order to achieve higher performance.

Spiegel et al. [4] used deep reactive-ion etching process to fabricate the serpentine microflow fields in the siliconwafer with the fuel cell channel widths and depths ranging from 20 to 200μm to compare with the conventional ones using traditional CNC machining processes with flow field channel dimensions of 500 and 1000μm. With the same MEA and percentage of active area (channel to rib ratio of 1:1), and under the same test conditions, the fuel cells could have the best performance with the 20-μm of width, depth and rib because such dimensions allowed increase of channel velocity, rapid diffusion and homogenous reactant distribution along the flow channel. Therefore, smaller flow channel dimensions (>100μm) appear to be promising for future micro fuel cell technologies.

Kim et al. [5] used photolithography, anisotropic wet etching, anodic bonding and physical vapor deposition to manufacture a miniaturized PEM fuel cell with silicon separators. A 400μm × 230μm flow channel was made with KOH wet etching on the front side of a silicon separator, and a 550nm gold current collector and 350nm TiNx thin film heater were respectively formed on the front side and the opposite side by PVD. Two separators were assembled with the membrane electrode assembly having

a 4cm^2 active area for the single cell. With pure hydrogen and oxygen under atmosphere pressure without humidification, the performance of the single fuel cell could lead to 203mW/cm^2 at 0.6V at room temperature.

Xiao et al. [6] fabricated a silicon/glass based micro fuel cell system by micromachining technique. The anode and cathode catalyst layers were formed by directly sputtering platinum on the ICP-etched (Inductively Coupled Plasma) high-aspect-ratio columns on silicon substrate. Integrated gold-based micro current collectors were patterned on the silicon and glass surfaces. The high-aspect-ratio columns effectively increased the catalyst surface area, and the micro pillars grown by their etching process further improved the cell performance.

Hsieh et al. [7] developed a novel design and microfabrication for a micro proton exchange membranes with a cross section area of 5cm^2 and thickness of about 800μm. It consisted of PMMA flow field plate with narrow and deep channel made by microsystem technology, platinum sputtering deposited on MEA, and an ultra thin copper layer again sputtering deposited on PMMA flow field plate used as a current collector. For the single cell, a reliable power output was obtained.

Hsieh et al. [8] also developed a SU-8 photoresist microfabrication process for micro proton exchange membrane fuel cell flow structures for both anode and cathode flow field plates with a cross section area of 5 cm2 and thickness of about 750μm. The new design for flow field plates would have SU-8 used not only a photoresist but also as a microstructure material. Their fabrication could make a low-cost and high-mass production of small flat single fuel cell with an acceptable power density

of about 30mW/cm2 at 0.35V.

Keyur et al. [9] firstly used polydimethylsiloxane (PDMS) as the substrate to fabricate the miniature hydrogen-air PEM fuel cell. In this work PDMS microreactors were fabricated by micromolding on the silicon mold made by photolithography and ICP etching process. Though the performances were still not competitive with standard ones, it did show the feasibility of producing micro PEM fuel cells by using the cheaper base substrates like PDMS in order to minimize their cost.

Song et al. [10] developed a simple and rapid method to fabricate planar PEM fuel cells in PDMS. They patterned a perfluorinated ion-exchange resin, such as a Nafion resin, on a glass substrate using a reversibly bonded PDMS microchannel to generate an ion-selective membrane between the fuel-cell electrodes.

Siu and Chiao [11] used PDMS as the material of gasket and electrode in microbial fuel cell. They used MEMS technology, such as etching and evaporation process, to form the microchannel pattern on the silicon wafer, and molding PDMS on the wafer. Compared with the recent silicon micromachined microbial fuel cell, their result showed the better performance in the average power density and average current density.

Different from the traditional "banded" way, Lee et al. [12] used the "flip-flop" method on the fuel cell stacks. They applied a variety of etching and deposition techniques adopted from microfabrication on glass and silicon substrates in two-cell and four-cell configurations. The current collection was achieved by pattering metal films on an insulating substrate. They found that film thickness is the dominant factor compared

to other parameters related to channel topology. Though this new idea can simplify the interconnect design, the fuel may become difficult to supply.

Zhang et al. [13] fabricated a 6-cell PEMFC stack combined with a small hydrogen storage canister. Each cell was made by sandwiching a membrane-electrode-assembly (MEA) between two flow field plates fabricated by a classical MEMS wet etching method using silicon wafer as the original material. The plates were made electrically conductive by sputtering a Ti/Pt/Au composite metal layer on their surfaces. The 6-cells lay in the same plane with a fuel buffer/distributor as their support, which was fabricated by the MEMS silicon–glass bonding technology. The performance obtained a peak power of 0.9W at 250mA/cm2.

Chen et al. [14] designed the 10-cell planar array stack (6cm×6cm× 0.9cm) and compared the performance of the parallel connected one to that of the serial connected one. They found that the parallel connected stack is better because it will not be affected by certain cell with worse performance, and both performances can be enhanced by force convection. They also found the uniformity of each individual cell in serial connected stack that using force convection is better than that using natural convection.

Kim et al. [15] used thin flexible printed circuit board (FPCB) as a current collector in order to reduce an air-breathing monopolar stack's volume. They also designed different patterns of the air-breathing holes on the cathode to find the effect of varying the geometry and opening ratios on stack performance. They found that in cathode the circular-hole pattern with opening ratio of 38% has the best performance, but also

causes cathode flooding and unstable output problems. And the rectangular cathode opening pattern with 65% opening ratio was chosen for high performance and voltage stability.

Cha et al. [16] observed the scaling effects of various flow channels in fuel cells with gaseous hydrogen/air reactants from macro feature size (>500μm) to micro one (<100μm). They found that scaling behavior is quite complicated due to highly non-linear convection both in the flow channels and porous electrode. Considering the model predictions, flooding issues, and pressure drop losses, the performance of interdigitated channels decreases as the feature size decreases. Therefore, a good compromise may be found between the reduced pressure drop and reduced performance at intermediate feature sizes depending on operation requirements.

Noponen et al. [17] introduced a measurement system for mapping of current distribution into a free-breathing polymer electrolyte membrane fuel cell. The result showed that the operating temperature has a significant influence on the fuel cell performance. Furthermore, at low cell temperatures the limiting factor is inadequate free convection, and at high temperatures it is drying. They also showed that under some condition this type of fuel cell has fairly homogenous current distribution and therefore does not need any auxiliary pumps or fans to increase the airflow.

Sun et al. [18] applied the technique of current density distribution measurement gasket to measure local current distribution in a PEM fuel cell with serpentine flow field at various humidification temperatures. Their experiments showed the following results: Whether the anode or

cathode, the performance or current density can reach the maximum when humidification temperature is equal to the cell temperature. Besides, when the anode and cathode humidification temperatures are equal, if the cell is highly under-humidified, then local current density starts very low and increases monotonously along the channel; if the cell is moderately under-humidified, then the local current density first increases, reaches a maximum, and then decreases along the channel; when the cell is well-hydrated or over-hydrated, the local current decreases monotonically along the channel.

Lee et al. [19] investigated the effect of changing the gas diffusion layer and bolt torque on the performance of a PEM fuel cell at fixed flow rates. The experiment results showed that brittle gas diffusion layer material has higher performance with a less bolt torque because the higher bolt torque may damage the diffusion layer. And when soft material is combined with the more brittle one, the same tendency can be observed. As a result, the bolt torque and the gas diffusion layer type are the important factors for performance of PEM fuel cell.

Fekrazad and Bergman [20] used a three-dimensional model of PEM fuel cell stack to predict the influence of nonuniform stack compression on thermal and electrical contact resistances at the BP-GDL. The result showed that the temperature distribution within the membrane is highly dependent on the clamping pressure distribution. Also, the application of nonuniform clamping pressure distributions can make thermal conditions within the stack to become more uniform. However, it has negligible impact on the fuel cell power output or maximum membrane temperature.

Lu and Reddy [21] combined the experimental and modeling

methods to investigate effects of different factors on the performance of the micro-PEM fuel cell (μ-PEMFC). Their results showed that among three types of resistance influenced by material, contact and thermal effects, contact resistance caused by the assembling mode of the μ-PEMFC contributes to 19.4% of the total inner resistance, which is much higher than the 2% of the others. Therefore, the designs of new flow field configurations and assembling modes are very important in improving the performance of μ-PEMFCs.

Lin et al. [22] investigated the gas permeability, bulk density, thickness and conductivity of two types of gas diffusion layer (OC14, NC14) as a function of the compressed thickness with an active area of 25 cm^2 in a single PEMFC. They found that increasing compression of gas diffusion layer can produce high-quality contact, but excessive compression will damage the carbon fiber, reducing the gas permeability and contact resistance. These results concerning the balance between compression and performance provide vital information for the fabrication of stacks and support for industrial applications.

Chang et al. [23] used a special-designed test rig to measure the thickness, gas permeability, and porosity of a GDL sample under various clamping pressure conditions. Their results showed that at low clamping pressure levels (e.g.< 5 bar), increasing the clamping pressure reduces the interfacial resistance between the bipolar plate and the GDL that enhances the electrochemical performance of a PEM fuel cell. In contrast, at high clamping pressure levels (e.g. >10 bar), although increasing the clamping pressure can reduce the above ohmic resistance, it also narrows

down the diffusion path for mass transfer from gas channels to the catalyst layers. Comprising the above two effects does not promote the power density too much but reduces the mass-transfer limitation for high current density.

Zhou et al. [24] developed a model to analyze the effects of assembly pressure, operating temperature and humidity on PEM fuel cell stack deformation, contact resistance, overall performance and current distribution. The modeling results revealed that elevated temperature and humidity enlarge gas diffusion layer and membrane inhomogeneous deformation, increasing contact pressure and reducing contact resistance due to the swelling and material property change of the GDL and membrane. When an assembly pressure is applied, the fuel cell overall performance is improved by increasing temperature and humidity. However, the stack would be more prone to degradation with significant variation of current distribution at elevated temperature and humidity.

Wen et al. [25] experimentally investigated the effects of various combinations of bolt configuration and clamping torque on the corresponding contact pressure distributions and performances of a single PEM fuel cell and a 10-cell stack. Their results showed that, for the single cell under the current experiment conditions, the larger mean contact pressure tends to yield the higher maximum power, regardless of the bolt configuration and the applied torque. The uniformity of the contact pressure distribution, the ohmic resistance and the mass transport limit current have highly linear correlations with the mean contact pressure. However, in the case of the 10-cell stack, the effects of various combinations of bolt configuration and clamping torque on its

performance and the mass transport limit current can not be reflected by the stack mean contact pressure only.

1.3 Scope of Present Study

In this thesis, it focuses on the flow field plate of a single micro PEMFC fabricated by using the MEMS technology to observe the feasibility of using PDMS as the material and combining both the gasket and flow field on the same plate. At first, two patterns were designed by AutoCAD to form the shape of flow field plate mold. Followed by several MEMS processes, the flow field plate mold was fabricated on a silicon wafer. And then PDMS molding process was taken to fabricate the PDMS flow field plate. Finally, a single PEMFC was assembled by flow field plates, acrylic plates, current collector slices and membrane-electrode-assembly (MEA). Then, a series of performance experiments on a single micro PEMFC were carried out. The research flow chart can be referred to Fig. 1-7. The experimental parameters include current collector shape, convection type, clamping force, respectively. After these experiments, it also connected several single PEMFCs, whose performance are close to the best one under the optimal combination of the parameters mentioned above, in series to form a cell stack, whose module is used to observe its performance.

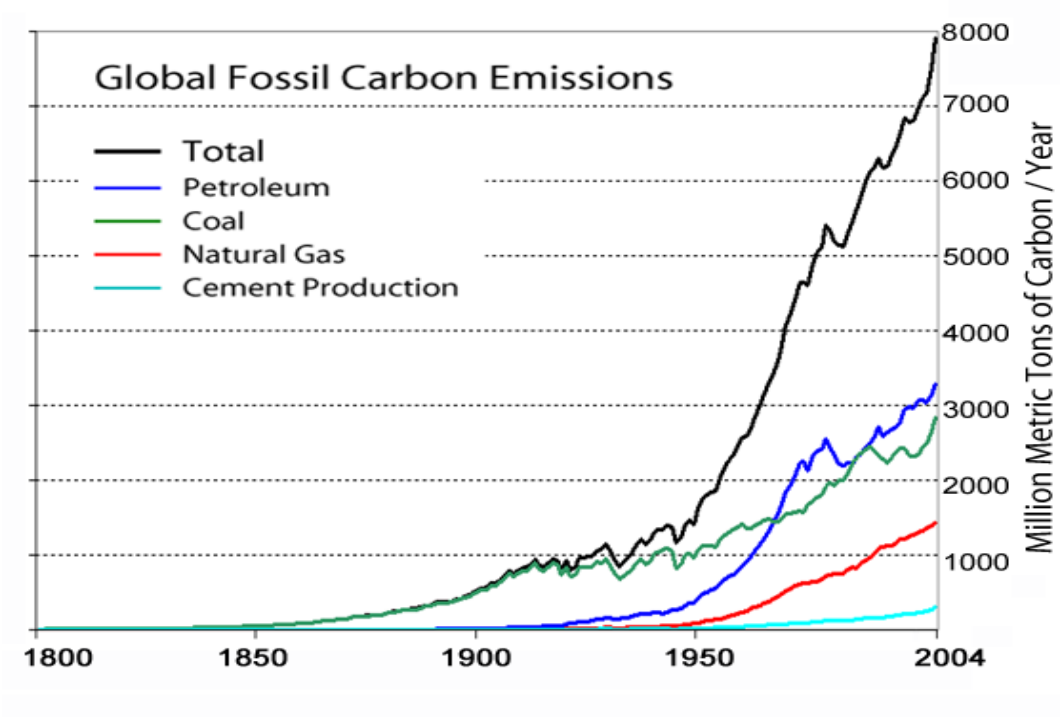

Fig. 1.1 Global Fossil Carbon Emissions in Recent Years
http://en.wikipedia.org/wiki/Greenhouse_gas

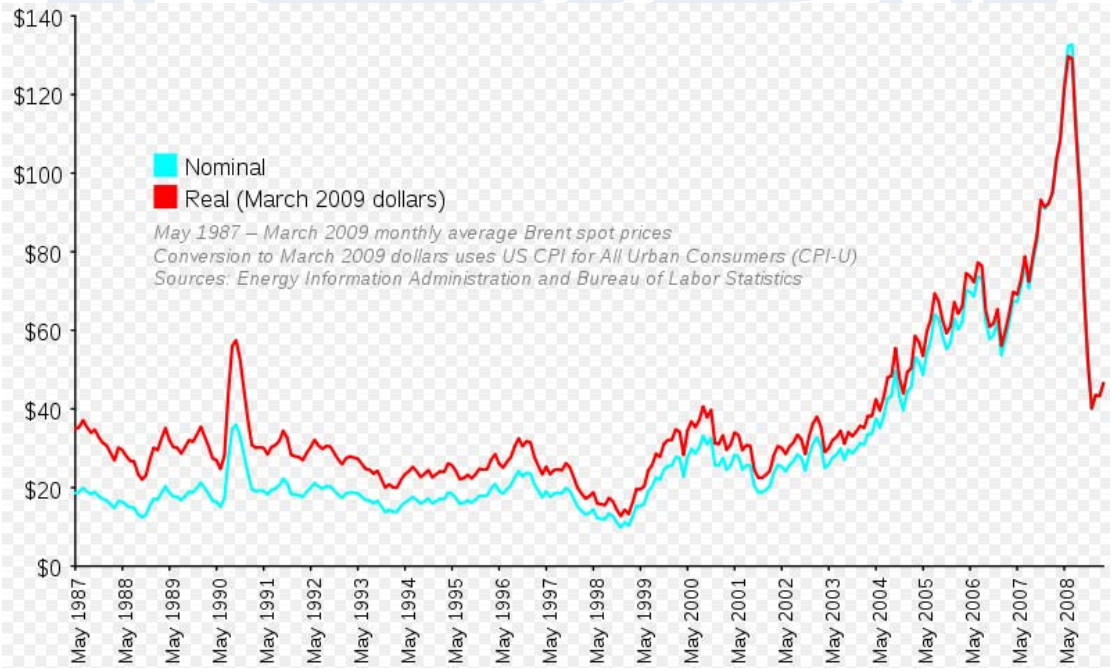

Fig. 1.2 The Petroleum's Price in Recent Year
http://en.wikipedia.org/wiki/Price_of_petroleum

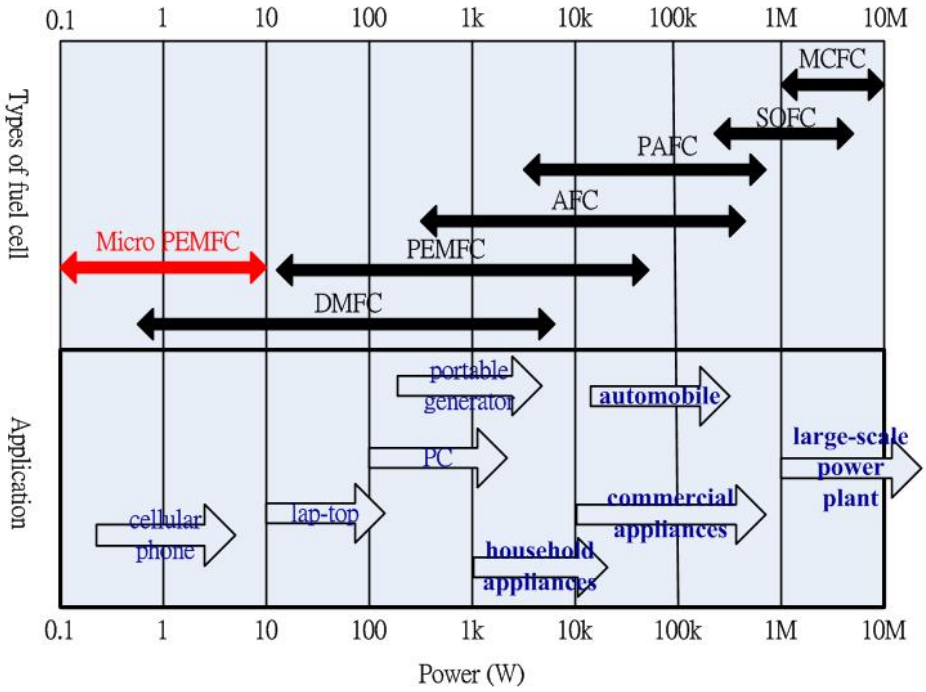

Fig. 1.3 Portable Power Sources, Ranged from KW to W

http://www.nhu.edu.tw/~society/e-j/63/63-32.htm

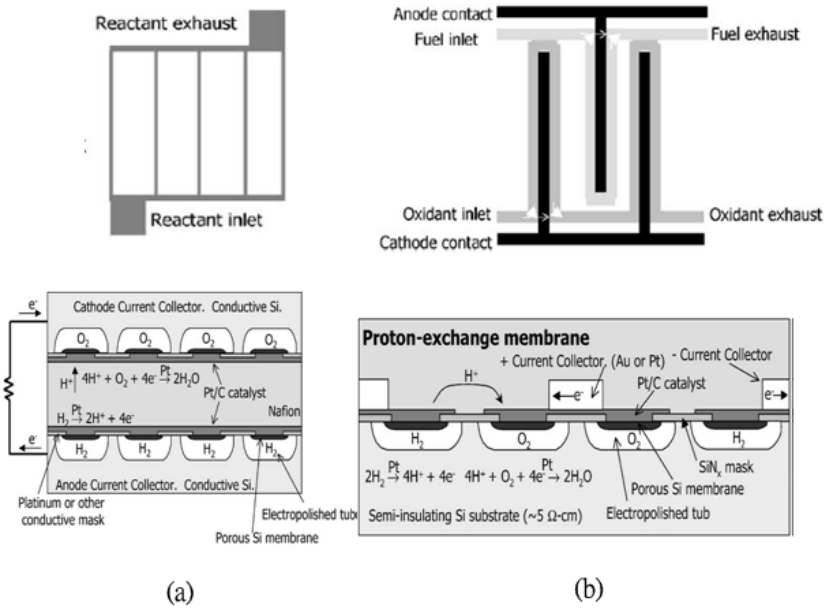

Fig. 1.4 (a) Bipolar Plate Design and (b) Monolithic Design [2]

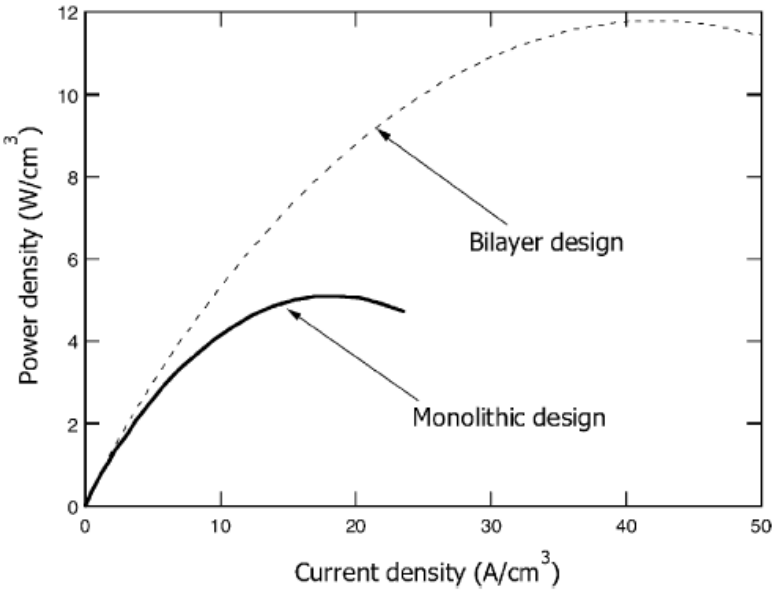

Fig. 1.5 Comparison of Power Densities for Bilayer and Monolithic Design [2]

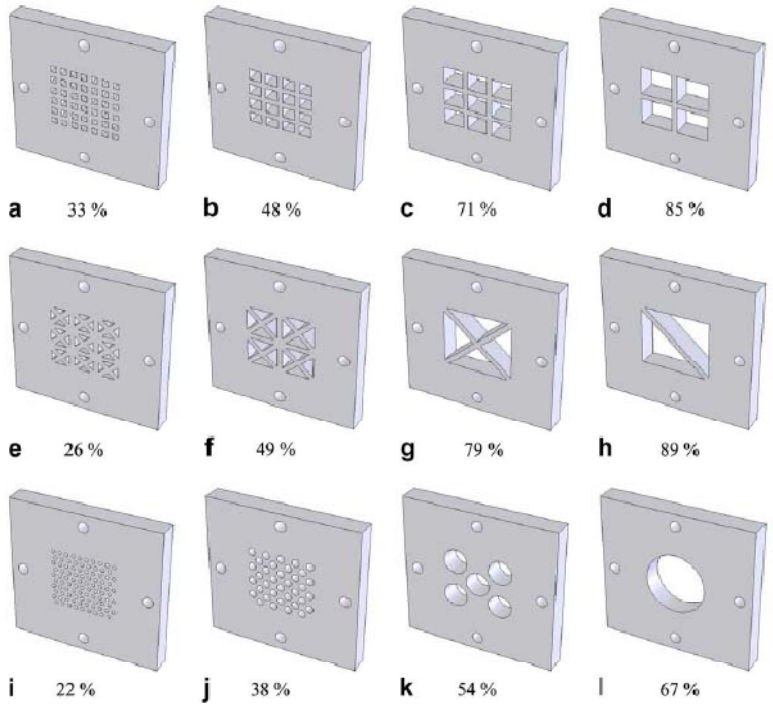

Fig. 1.6 Unit Cell Cathode Plate Designs for the Rectangular, Triangular and Circular Opening Geometries at Various Opening Ratios [15]

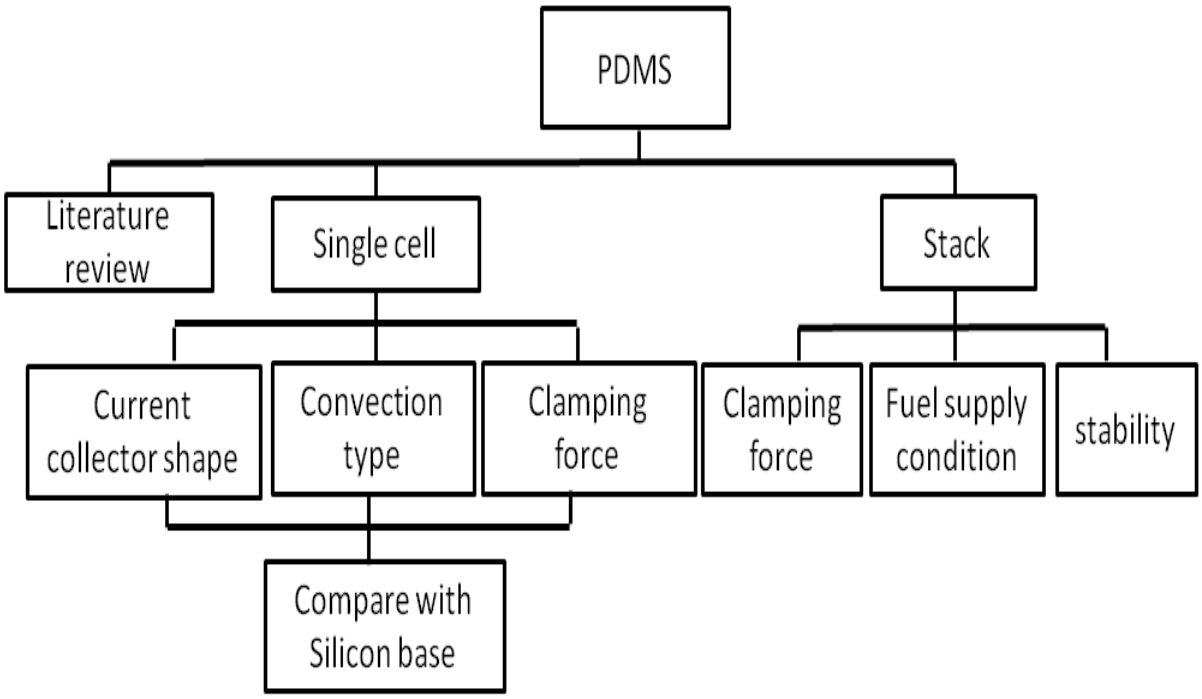

Fig. 1.7 Research Flow Chart

Chapter 2

Fundamentals of Fuel Cell

2.1 History of Fuel Cell:

The first demonstration of a fuel cell was by a lawyer and scientist William Grove in 1839, using the reverse experiment that water is being electrolyzed into hydrogen and oxygen. And it did generate a small current that constructs the first concept of fuel cell. Not until 1889, Mond and Langev utilized precious metal, Pt, as the catalyst to develop the first cell under the Grove's conception such that the formal words of "fuel cell" came up. At that time, their cell could generate 3.5mA/cm2 at 0.7V.

In 1932, Francis Bacon used alkaline electrolyte and Ni as the catalyst to replace Pt to fabricate the alkaline fuel cell different from Mond and Langer's one. After 27 years, both Bacon and Allis-Chalmers company invented the machines powered by fuel cells. These developments helped the commercialization for fuel cell in the future.

During 1960 to 1970, NASA used the fuel cell as the main power source of the spacecraft because its power deliver of 1~10kW was right fit the astronautic need plus the produced water could supply drink to astronauts in the outer space. The development program continued with the invention of a new polymer membrane called Nafion, a registered trademark of DuPont, in 1967. Even after 50 years, however, the cost of manufacture and materials are still too expensive for fuel cells to let them be popular in commercialization. There are still some difficulties to be solved. Fortunately, owing to the mature development of fabrication technologies of MEMS and NANO, the fuel cell now can be minimized

into micro scale that can be applied in lots of electronic products.

2.2 Principle of the Fuel Cell

2.2.1 Thermodynamics

Fuel cell is more efficient than heat engines because it converts chemical energy to electrical energy directly. Carnot cycle shows the possible maximum efficiency of a heat engine, which can be expressed as:

$$\eta = \frac{T_H - T_L}{T_H} \quad (2\text{-}4)$$

where TH is the maximum temperature and TL is the rejection temperature of the heat engine. For a typical heat engine that operates at 675K and rejects heat at 325k, the Carnot efficiency limit is 52%.

The ideal efficiency of a fuel cell is given by the ratio of the thermodynamically extractable energy of the reaction to the total heat energy that would have been released by the reaction in combustion:

$$\eta = \frac{\Delta G}{\Delta H} \quad (2\text{-}5)$$

At standard conditions, ΔH0 for the hydrogen/oxygen reaction is -285.83KJ/mole and ΔG0 is -237.14KJ/mole, giving a theoretical efficiency limit of 83%.

Although ΔG0 represents the energy potential that can be extracted by a fuel cell at standard condition, this energy is expressed by the fuel cell as an electrical potential, or voltage (E0):

$$E_0 = \frac{\Delta G^0}{2F} \quad (2\text{-}6)$$

At standard conditions, this equation gives 1.23V, which is referred as the fuel cell open circuit voltage (OCV).

ΔG is a function of temperature and pressure, therefore, the fuel cell open circuit voltage changes depending on the operating conditions. These dependencies are described by the Nernst equation:

$$E_{Nernst} = E_0 + \frac{RT}{2F} \ln \frac{P_{H_2} P_{O_2}^{\frac{1}{2}}}{P_{H_2O}} \quad (2\text{-}7)$$

The ideal fuel cell voltage decreases with increasing temperature, but usually the opposite trend is true for the actual fuel cell efficiency due to accelerated electrochemical reaction kinetics at higher temperatures.

2.2.2 Kinetics

An ideal fuel cell would supply an infinite current while maintaining the constant voltage determined by the Nernst equation. But in fact, the actual voltage output of a real fuel cell is less than the ideal thermodynamically predicted voltage. Furthermore, the more current is drawn from a real fuel cell, the more the voltage output of the cell declines, limiting the total power that the fuel cell can deliver. The performance of a real fuel cell device can be summarized with a graph of its current versus voltage characteristics. Such graph, called an I-V curve, shows the real voltage output of the fuel cell for a given current output. An example of a typical I-V curve for a PEMFC is shown in Fig. 2.1.

The voltage output of a real fuel cell is less than the thermodynamically predicted voltage output due to irreversible kinetic losses. The more current is drawn from the cell, the greater these losses. There are three major types of fuel cell losses, which give a fuel cell I-V curve to its characteristic shape as shown in Fig 2.2:

1. Activation losses
2. Ohmic losses
3. Concentration losses

An equation for the true fuel cell I-V behavior can thus be written by starting with the thermodynamically predicted voltage output of the fuel cell and then subtracting off the various loss terms:

$$E_{real} = E_{Nernst} - \eta_{act} - IR - \eta_{conc} \quad (2\text{-}8)$$

These three categories of irreversibility are considered one by one in the following sections.

2.2.2.1 Activation Losses

At low current density, the voltage of a fuel cell drops rapidly because of the sluggishness of the electrochemical half reactions occurring at the anode and the cathode electrodes. The oxygen reduction reaction at the cathode is especially sluggish and can account for most of the activation losses. Although the final state of product water is lower in energy than that in the initial reactants, an energy barrier impedes the conversion of reactants into products. A portion of the fuel cell voltage is sacrificed to lower this barrier and thus increases the rate at which reactants are converted into products, allowing the fuel cell to output more current. The relationship between the applied activation overvoltage and the current density output is exponential in nature, and can be described by the Butler-Volmer equation:

$$i = i_0 \left(\frac{C_O}{C_O^*} e^{-\frac{\alpha F \eta_{act}}{RT}} - \frac{C_R}{C_R^*} e^{-\frac{(1-\alpha) F \eta_{act}}{RT}} \right) \quad (2\text{-}9)$$

When the overvoltage is greater than 50mV, the Butler-Volmer

equation can be approximated by a much simpler form, called the Tafel equation:

$$\eta_{act} = \frac{RT}{\alpha F} \ln \frac{i}{i_0} \tag{2-10}$$

Activation losses are minimized by maximizing the exchange current density. The exchange current density is a function of the catalyst material and the total reaction surface area. As mentioned earlier, the electrodes are highly porous to maximize the total reaction surface area. Highly dispersing, nano-scale particles of platinum are mixed into the porous electrode so that they are in intimate contact with the gas phase pores, the electrically conductive electrode, and the ion conductive electrolyte. This maximizes the amount of triple phase boundary, thus maximizing the exchange current density. Platinum is currently the best known catalyst for PEMFC.

2.2.2.2 Ohmic Losses

Ohmic losses arise due to the internal resistance of the materials in the fuel cell to the flow of electrons and protons. These losses are called "Ohmic losses" because they generally follow Ohms law, V=IR. Both the electrically conductive electrodes and the ion conductive electrolyte contribute to the resistance losses. Usually, ionic resistance is dominant in a well-designed fuel cell. The linear drop in the middle of the I-V curve in Fig. 2.3 distinctly manifests the Ohmic loss effects. In fuel cell systems, most of the Ohmic loss arises from the electrolyte.

2.2.2.3 Concentration Losses

At high current density, the voltage output of fuel cell once again drops rapidly and declines quickly to zero. The current density output at

zero voltage is known as the short-circuit current, which represents the maximum current that can be produced by the fuel cell. However, at this current level, the voltage output of fuel cell is zero, so the total power delivered by the fuel cell is also zero. Therefore, power peak occurs somewhere in the middle of the I-V curve. The reason for the final steep decline in fuel cell voltage at high current density is due to mass transport limitations. At high current density, the fuel or the oxidant gases are consumed on the reaction surfaces faster than they can be replenished. At a certain limiting current density, the partial pressures of the reactant gases at the reaction surfaces plummet towards zero. From the Nernst equation, it is clear that this dramatic decline in the partial pressures of reactants causes a dramatic decline in output voltage. The voltage drop from this mass transportation limit is:

$$\eta_{conc} = A \ln\left(1 - \frac{i}{i_l}\right) \quad (2\text{-}11)$$

where A is a fitting parameter (V) and it is obvious that the concentration loss is dominant at high current density. Well-designed flow structures and thin, highly porous electrodes may reduce the concentration overvoltage.

2.3 Type of Fuel Cells

There are five major types of fuel cells as follows.

1. Solid Oxide Fuel Cell (SOFC)
2. Molten Carbonate Fuel Cell (MCFC)
3. Phosphoric Acid Fuel Cell (PAFC)
4. Alkaline Fuel Cell (AFC)
5. Proton Exchange Membrane Fuel Cell (PEMFC)

While all five fuel cell types are based upon the same underlying electrochemical principles, they all operate at different temperature regimes, incorporate different materials, and often differ in terms of their fuel tolerance and performance characteristics. These are shown in Table 2.1.

Table 2.1 The Five Major Types of Fuel Cells [26]

Type of fuel cell	**PAFC**	**MCFC**	**SOFC**	**PEMFC**	**AFC**
Electrolyte	H_3PO_4	$(Li,K)_2CO_3$	$(Zr,Y)O_2$	MEA	Polymer
Anode	Pt/C	Ni+10wt%Cr	$Ni+(Zr,Y)O_2$	Pt/C, Pt-Ru/C	Pt/C
Cathode	C	NiO	$(La,Sr)MnO_3$,$LaCoO_3$	Pt/C	Pt/C
Ion	H^+	CO_3^{2-}	O^{2-}	H^+	OH^-
Reaction of anode	$H_2 \rightarrow 2H_2O+ 2e^-$	$H_2+CO_3^{2-} \rightarrow H_2O+CO_2+2e^-$	$H_2+O^{2-} \rightarrow H_2O+2e^-$ $CO+O^{2-} \rightarrow CO_2+2e^-$	$H_2 \rightarrow 2H_2O+ 2e^-$	$H_2 + 2OH^- \rightarrow 2H_2O+ 2e^-$
Reaction of cathode	$1/2O_2+2H^++ 2e^- \rightarrow H_2O$	$1/2O_2+CO_2+2e^- \rightarrow CO_3^{2-}$	$1/2O_2+2e^- \rightarrow O^{2-}$	$1/2O_2+2H^++ 2e^- \rightarrow H_2O$	$1/2O_2+2H_2O+ 2e^- \rightarrow 2OH^-$
Operating temperature	160~190°C	600~700 °C	900~1,000 °C	30~80 °C	90~100 °C
Fuel compatibility	H_2	H_2, CH_4	H_2, CH_4, CO	H_2, methanol	H_2
Advantage	CO durability, combined heat and power	high power, combined heat and power, reform the fuel in cell	high power, combined heat and power, air as oxidant, reform the fuel in cell	high density power, air as oxidant, operating in room temperature, fast activation,	Operating in room temperature, fast activation
Disadvantage	operating in high temperature, high cost, low efficiency	device can be corroded	operating in high temperature, damaging in high temperature	high cost, infecting by CO	high cost, fuel is only H_2
Application	distributed generation	large-scale power plant, distributed generation	large-scale power plant, distributed generation, automobile industry	domestic appliances, portable source, automobile	spaceship

2.3.1 SOFC

Solid oxide fuel cell (SOFC) is a complete solid-state device that uses an oxide ion-conducting ceramic material as the electrolyte, and includes a lanthanum manganate cathode and a nickel zirconia anode. SOFC works in the region of 800 to 1100℃. This means that high reaction rates can be achieved without expensive catalysts, and that gases such as natural gas can be used directly, or "internally reformed" within the fuel cell, without the need for a separate unit. This type of fuel cell addresses all the problems and takes full advantage of the inherent simplicity of the fuel cell concept. Therefore, it is a promising option for high-powered applications, such as industrial uses or central electricity generating stations.

2.3.2 MCFC

The electrolyte of the molten carbonate fuel cell is a binary molten mixture of lithium and potassium, or lithium and sodium carbonates. It has the potential to be fueled with coal-derived fuel gases or natural gas. Unlike the other fuel cells, carbon dioxide must be supplied to the cathode, and thus converted to carbonate ions. The high temperature achieves a good reaction rate by using a comparatively inexpensive catalyst-nickel. Therefore, MCFC is also a high-temperature fuel cell like SOFC.

2.3.3 PAFC

The phosphoric acid fuel cell (PAFC) uses a phosphoric acid as an electrolyte to conduct proton which is like Nafion membrane in the PEMFC. In PAFC, the electrochemical reactions take place on highly

dispersed electrocatalyst particles supported on carbon black. Phosphoric acid is the inorganic acid that has high thermal, chemical, and electrochemical stability. It also contains high volatility (above 150℃) to be adopted as an electrolyte for fuel cells. Due to its low freezing point (42℃) of the pure phosphoric acid, PAFC is usually maintained above such temperature. Unlike PEMFC, the operating temperature of PAFC is normally around 180 to 200℃ that has greater tolerance of CO (up to 1%). PAFC is the first one to be produced in commercial quantities and enjoys widespread terrestrial use.

2.3.4 AFC

The electrolyte of the alkaline fuel cell is an alkaline solution, such as potassium hydroxide, and is operated at about 200℃. AFC is used by NASA on spacecraft, and it is now finding new applications in hydrogen-powered vehicles.

2.3.5 PEMFC

The proton exchange membrane fuel cell capitalizes on the essential simplicity of the fuel cell. The electrolyte is an ion conduction polymer to move H+ ion pass through the supporting ionomer structure. PEMFC appears to be more adaptable to automobile use than PAFC. PEMFC works at low temperature which can start quickly. The thinness of the MEA makes the compact design without corrosive fluid in the fuel cell. These cells are the best candidates for light-duty vehicles, buildings, and much smaller applications. A very attractive solution to the hydrogen supply problem is to use methanol as a fuel instead. Such cell is called

direct methanol fuel cell (DMFC). It also uses a polymer membrane as an electrolyte.

The thesis is interested in state-of-the-art PEMFC science and technology, because it is simple structure, runs at relatively low temperature, widely practicability and high efficiency.

2.4 Fuel Cell Stack

The voltage of a single fuel cell is fixed by its particular electrochemical reaction, about 0.7V when drawing a useful current. This means that to produce a useful voltage many cells have to be connected in series. Such a collection of fuel cells in series is known as a "stack". The stack design and number of single cell depend on the power needed.

2.5 Principle of PEMFC

PEM fuel cells use a proton-conducting polymer membrane as an electrolyte. They are low temperature fuel cells, generally operating at 85-105℃. The reaction in a PEM fuel cell are the same as in a PAFC as they both employ an acidic electrolyte Equations (2.1) and (2.2). The anode reaction consists of hydrogen oxidation to protons; the protons migrate through the membrane to the cathode. At the cathode, oxygen is reduced and then recombines with the protons to form water.

$$\text{Anode: } H_2 \xrightarrow{Pt} 2H^+ + 2e^- \quad (1\text{-}1)$$

$$\text{Cathode: } \frac{1}{2}O_2 + 2H^+ + 2e^- \rightarrow H_2O + Heat \quad (1\text{-}2)$$

$$\text{Overall: } H_2 + \frac{1}{2}O_2 \rightarrow H_2O + Heat \quad (1\text{-}3)$$

Different from the conventional battery, the fuel cell is a device that transforms chemical energy into electricity that does not participate in the

reaction. As the active material stored in fuel cell is used up, the device must be stop using and resupplied with the chemical material to work; in other word, the fuel cell is just a transformation machine.

2.6 Structure of PEMFC

A PEMFC, shown in Fig. 2.4, is simply like a sandwich structure. Each component is described as follows:

2.6.1 Bipolar Plate, Current Collector, and End Plate

In a single fuel cell stack, several fuel cells are assembled in series. The bipolar plate is the electronically conductive plate positioned next to the anode end of one cell and the cathode end of another cell. In general, each surface of the bipolar plate contains grooved channels with inlet and outlet as flow path of the fuel and oxidant, respectively. The current collectors are next to the bipolar plates to collect the electric current and connect to the outside load. The end plates keep all the parts of the cell fixed.

2.6.2 Gas Diffusion Layer (GDL)

The gas diffusion layer (GDL) is usually made of carbon paper or cloth with a porous structure treated with hydrophobic agent. It has to meet several requirements, such as electronic conductivity, heat conductivity, fluid permeability, wet ability, and mechanical stability.

2.6.3 Gasket

The gasket is made of Teflon-PTFE, whose characteristics are able to endure the high temperature, corrosion, and etc. It also can avoid the gas spreading out from the gas diffusion layer (GDL) because GDL has a

thickness. So the gasket plays an important role in sealing.

2.6.4 Proton Exchange Membrane (PEM)

The “core” of a fuel cell comprises a solid perfluorsulphonic acid polymer, usually named as Nafion from DuPont. It functions as a path for protons. The protons are transferred by migration and convection with water. The membrane, therefore, not only needs to be maintained hydrous but also is free from flooding.

2.6.5 Active Layer

The active layer contains the porous catalyzing material and is positioned between PEM and GDL. For a PEMFC, active layer is usually the platinum (Pt) metal in the anode and cathode. The function of Pt metal is to activate the electrochemical reactions.

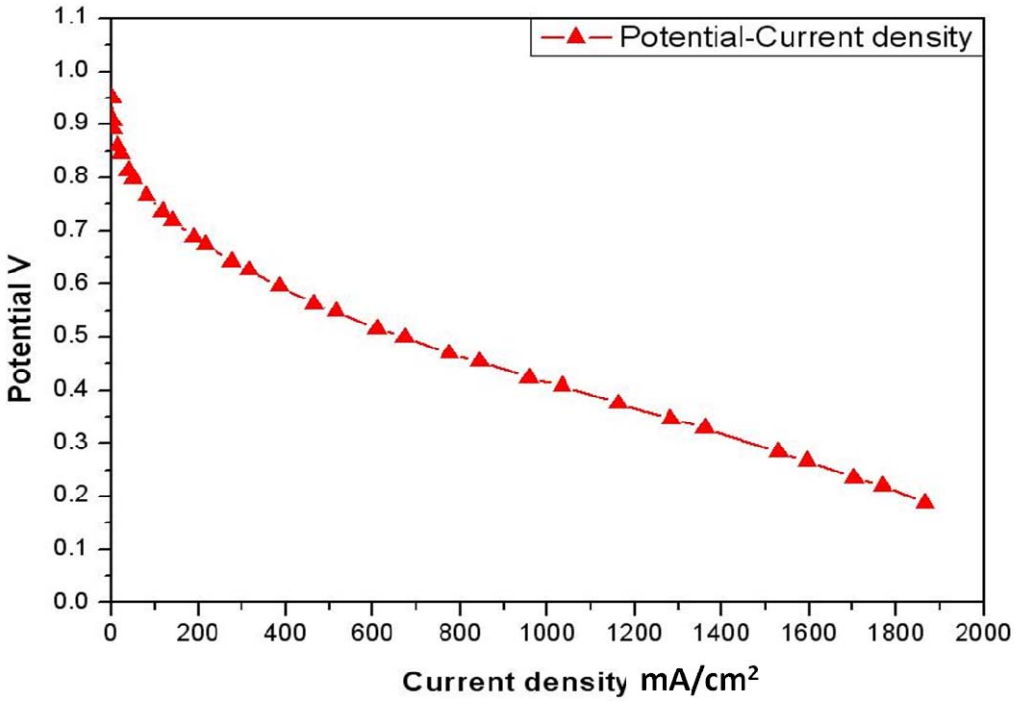

Fig. 2.1 Typical *I-V* Curve For a PEMFC

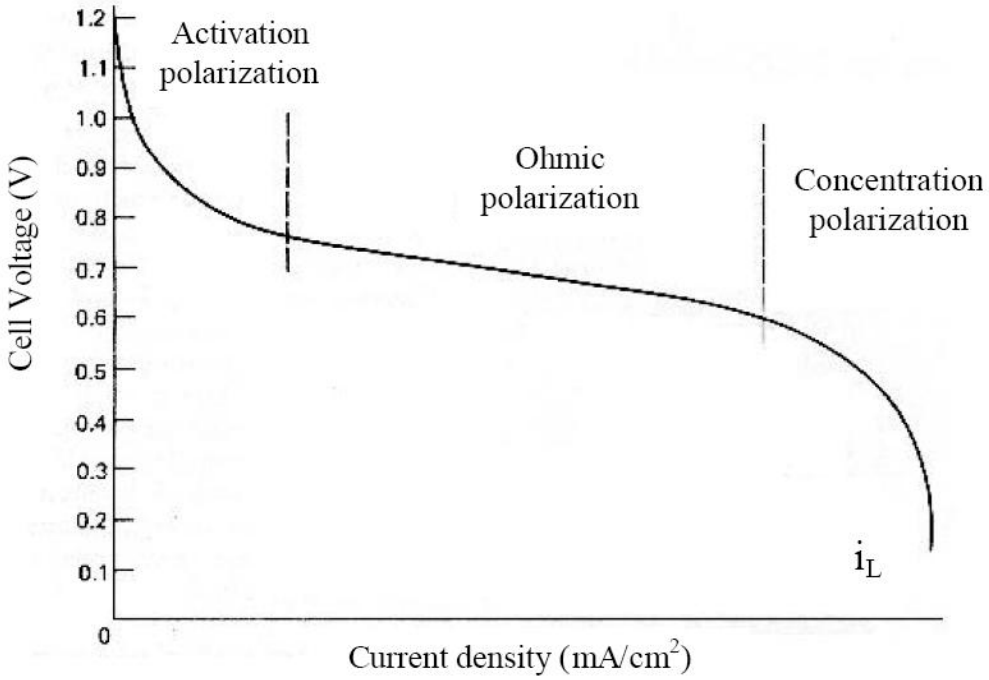

Fig. 2.2 I-V Curve of Fuel Cell

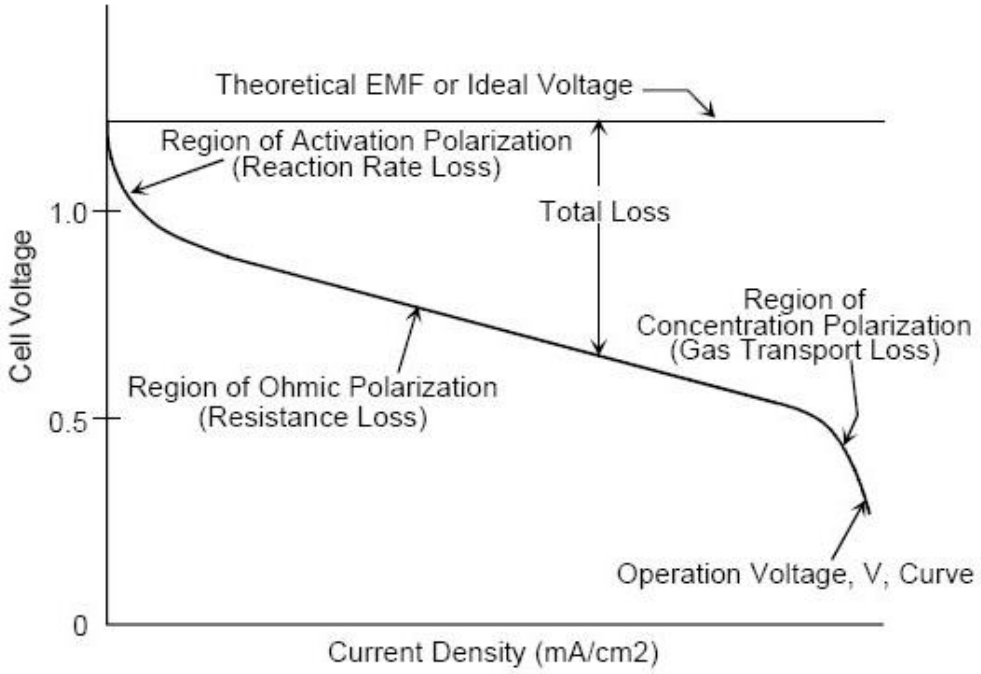

Fig. 2.3 Linear Drop in the Middle of the I-V Curve

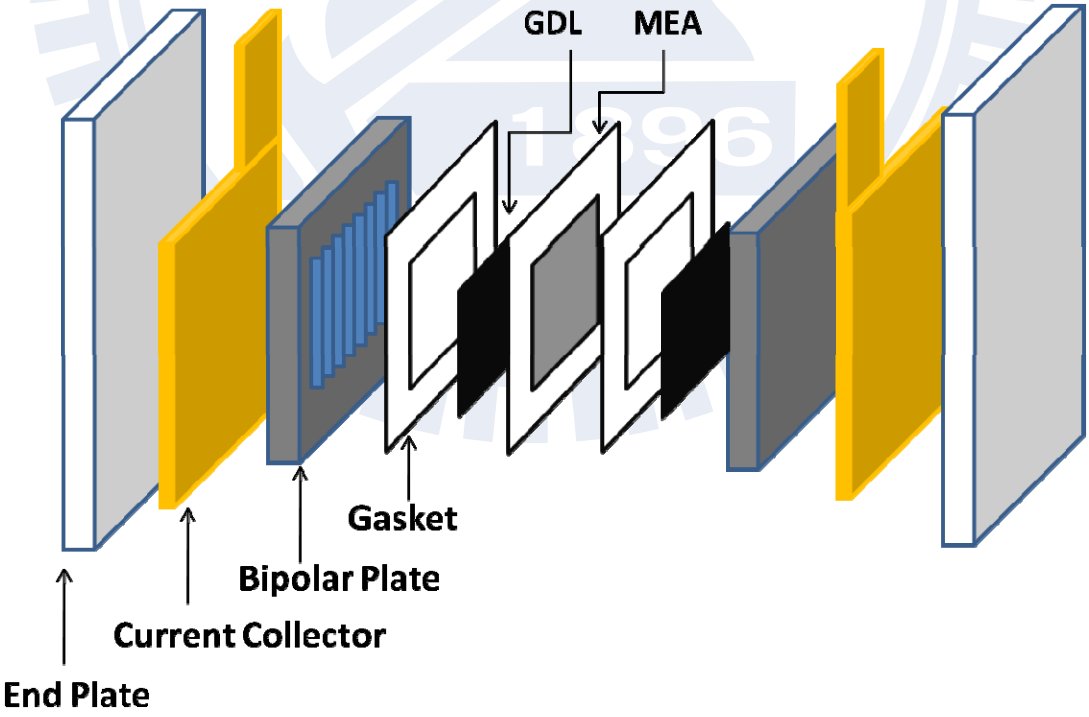

Fig. 2.4 Sandwich Structure of PEMFC

Chapter 3

Experimental Apparatus and MEMS Fabrication Processes

3.1 Processes of Fabricating the Flow Field Plates

The fabrication of micro PEMFC is different from the conventional way, especially in the flow field plate. Instead of being manufactured by machine tool like CNC, the micro PEMFC adopts the MEMS fabrication. The overall fabrication includes two processes: (1) process of fabricating silicon flow field mold; (2) process of micromolding PDMS on silicon flow field mold. Figure 3.1 shows the steps of fabrication process for flow field plate, and the details are given as follows:

3.1.1 Mask Design

The mask is designed by AutoCAD. In this work, it designs the flow field plate combining with the gasket on the same plate. The flow field plates should have different heights on different patterns, so it needs two different masks to complete the whole pattern, including the edge part (the gasket part), and the flow channel part. The area of flow field is about 3cm2 (1.7cm×1.7cm); see Fig. 3.2.

3.1.2 RCA Clean

The RCA (Radio Corporation of America) clean, as shown in Table 3.1, in the wet bench (Fig. 3.3) is a standard set of wafer cleaning steps which needs to be performed before the high-temp processing steps (oxidation, diffusion, CVD) of silicon wafers in semiconductor manufacturing. Werner Kern developed the basic procedure in 1965 while working for

RCA, the Radio Corporation of America. It involves the following steps:

I. Removal of the organic contaminants (Caro Clean)

II. Removal of thin oxide layer (Oxide Strip)

III. Removal of the organic contaminants (Organic Clean)

IV. Removal of ionic contamination (Ionic Clean)

V. Spin drying, see Fig. 3.4.

Table 3.1 the Steps of RCA Clean Process

Steps	***Title***	***Chemical solution***	***Experimental parameter***	***Function***
1	Caro System	H_2SO_4：H_2O_2=3：1	Temperature:120℃ Drenching:600sec	Removal of insoluble organic contaminants
2	Clean	D.I. water	Temperature: room temperature Time:60sec	Clean
3	DHF (Diluted HF)	HF：H2O = 1：50	Room temperature	Removal of thin oxide layer
4	Clean	D.I. water	Temperature: room temperature Time:60sec	clean
5	SC 1 System	NH_4OH：H_2O_2： H_2O=1：1：5	Temperature:75℃ Drenching:600sec	Removal of the organic contaminants
6	Clean	D.I. water	Temperature: room temperature Time:60sec	Clean
7	SC 2 System	HCL：H_2O_2： H_2O=1：1：6	Temperature:75℃ Drenching:600sec	Removal of ionic contamination
8	Clean	D.I. water	Temperature: room temperature Time:60sec	Clean
9	Spin drying		Step1：1200rpm;time:120sec Step2：1800rpm;time:150sec	Spin drying

3.1.3 Deposition of block layer Al

To protect Si substrate from the later step of ICP etching process, it deposits Al thin film about 300nm by the sputter (see Fig. 3.5) as a block layer at first. Sputter deposition is a method of depositing thin films by sputtering, driven by momentum exchange between the ions and atoms in the material due to collisions. Ions in the plasma are accelerated by the electric field between two electrodes, causing the ion bombardment, and sputter the atoms on the target, e.g., Al. Then sputtered atoms are ejected into the gas phase plasma and transferred to the substrate by diffusion to complete deposition.

3.1.4 Fabrication of Photolithography (the first mask)

The step is important in the all of fabrication processes to define the pattern, which it uses the first mask to form the edge side of flow channel plate mold that should be etched at the next two steps, such as Al and ICP etching. It is fabricated by Track MK-8 (Fig. 3.6), whose functions include coating PR (photo resist), exposure, development processes. This is a serial process which can lower the experimental uncertainty in the pattern work. Table 3.2 shows the parameters of Track MK-8.

Table 3.2 Parameter of Track MK-8

Wafer flow No	***Function***	***Step 1***	***Step2***	***Step3***	***Step 4***	***Step5***	***Step6***
1	NEB Resist Coatiog	Unit Cassette 1-1,1-2,1-3, 1-4	AD(2-3) 90℃	COL(2-6) 23℃	COAT(2-1) 4400rpm	HP(2-8) 110℃, 120sec	Unit Cassette 1-1,1-2,1-3, 1-4
2	DSE Resist Coating	Unit Cassette 1-1,1-2,1-3, 1-4	AD(2-3) 90℃	COL(2-6) 23℃	COAT(2-1) 2000rpm	HP(2-8) 95℃, 120sec	Unit Cassette 1-1,1-2,1-3, 1-4
8	G-line Resist Coating	Unit Cassette 1-1,1-2,1-3, 1-4	AD(2-3) 90℃	COL(2-6) 23℃	COAT(2-1) 5000rpm	HP(2-8) 90℃, 60sec	Unit Cassette 1-1,1-2,1-3, 1-4
20	I-line Resist Coatiog	Unit Cassette 1-1,1-2,1-3, 1-4	AD(2-3) 90℃	COL(2-6) 23℃	COAT(2-1) 3435rpm	HP(2-8) 90℃, 90sec	Unit Cassette 1-1,1-2,1-3, 1-4
5	NEB Resist Develop	Unit Cassette 1-1,1-2,1-3, 1-4	HP(2-4) 105℃, 120sec	COL(2-9) 23℃	DEV(2-2) 60sec	DHP(2-7) 110℃, 120sec	Unit Cassette 1-1,1-2,1-3, 1-4
4	DSE Resist Develop	Unit Cassette 1-1,1-2,1-3, 1-4	HP(2-4) 115℃, 120sec	COL(2-9) 23℃	DEV(2-2) 60sec	DHP(2-7) 115℃, 60sec	Unit Cassette 1-1,1-2,1-3, 1-4
11	G-line Resist Develop	Unit Cassette 1-1,1-2,1-3, 1-4	HP(2-5) 120℃, 60sec	COL(2-9) 23℃	DEV(2-2) 60sec	DHP(2-7) 120℃, 90sec	Unit Cassette 1-1,1-2,1-3, 1-4
21	I-line Resist Develop	Unit Cassette 1-1,1-2,1-3, 1-4	HP(2-4) 110℃, 60sec	COL(2-9) 23℃	DEV(2-2) 60sec	DHP(2-7) 120℃, 90sec	Unit Cassette 1-1,1-2,1-3, 1-4

3.1.5 Removing the Block Layer Al

This step is to define the pattern that should be etched by the next step of ICP etching. The block layer of Al is etched by Al etchant under a etching rate of 660nm/min.

3.1.6 Dry etching of Si

After removing Al, the wafer can be dry etched by the inductively coupled plasma (ICP) etcher (see Fig. 3.7). ICP is a type of high density plasma source in which the energy is supplied by electrical currents, produced by electromagnetic induction, that is, by time-varying magnetic fields. Its advantages are the high aspect ratio and the higher etching speed than the low density plasma one. The process of ICP etching contains four steps in one cycle: (1) Increase the flow rate of C_4F_8 gas to form a polymeric passivation layer on the surface and sidewall of the structure. Meanwhile the ion bombardment of Ar^+ keeps working in this step and also in the second and third ones. (2) Decrease the flow rate of C_4F_8 and gradually increase the one of SF_6 gas. This step is to etch the passivation layer on the structure surface, helping the third step of deep etching. (3) Shut down the flow of C_4F_8 and increase intensively the SF6 gas flow rate. The fluorine ion, F^+, tends to react with Si, forming evaporable compound which can be drained away by the vacuum to complete the etching process.

3.1.7 Strip (Remove PR)

For the positive photo resist, removing the remaining PR not used is called strip. Two ways of stripping are often been utilized: wet and dry. For wet stripping, organic solution like acetone or inorganic solution like

vitriol and hydrogen peroxide are being used. However, the inorganic solution will react with the metal, so in this step it adopts the acetone for stripping.

3.1.8 Repeat 3.1.4~3.1.7 with the second mask

The second mask is mainly used to form the flow channel part. The following steps are nothing different from the steps mentioned previously that include the Photolithography, removing the Block Layer Al, dry etching the Si, and strip. The silicon flow field plate mold is done after all these fabrication processes are finished (Fig. 3.8).

3.1.9 Micromolding PDMS on the silicon flow field mold

The molding process takes advantage of the fact that PDMS is a fluid at room temperature that is easily converted into solid form by cross-linking upon heating. To begin the molding process, a premixed substance of 10:1 weight ratio of Sylgard polymer base and curing agent is slowly poured on the silicon mold wafer, and then the wafer is put into the vacuum chamber (see Fig. 3.9). After degassing for 1 hour to remove bubbles before curing, the PDMS is cured at 60℃ for 2 hours and peeled-off from the wafer. Now several PDMS flow field plates are completed and they are cut into several individual ones with razor blade. (See Fig. 3.10)

3.2 Assembly and Components of micro PEMFC

3.2.1 Components of Micro PEMFC

For a Micro PEMFC, its components include Membrane Electrode Assembly (MEA), Gas Diffusion Layer (GDL), Current collector slices, Flow field plate, and Acrylic plate. Some of them have to be done extra works. For examples, the flow field plates need to be drilled gas inlet and outlet before assembly, and the acrylic plate in air-breathing cell needs an extra hole for natural convection. These components are shown in Figs. 3.11, and 3.12.

3.2.2 MEA and GDL

The MEA used is manufactured by the Asia Pacific Fuel Cell Technologies. Fig. 3.11 shows the picture of the MEA and GDL. Its specifications are listed in Table 3.3.

Table 3.3 The properties of MEA

MEAs DupPont^{TM} Nafion® NRE-212	
Anode Loading (Pt)	0.3 (mg/cm^2)
Cathode Loading (Pt)	0.5 (mg/cm^2)
Active area	4cm^2 (2cm × 2cm)

3.2.3 Assembly of Micro PEMFC

The single micro PEMFC is assembled by bipolar plates, acrylic plates, current collector slices and membrane-electrode-assembly (MEA). The shape of the structure is like sandwich, as shown in Figs. 3.13 and 3.14. Because such micro PEMFC uses forced convection to transport oxidant (air or pure oxygen) and hydrogen, the sealing problem must be

treated carefully.

3.2.4 Different Shapes of Current Collector Slices

The current collector is an important parameter affecting the micro PEMFC performance, so five different shapes of current collector slices under the same open ratio (the rate of the non-conductive area and the total) are designed. The material used is gold-plated copper. (Fig. 3.15)

3.2.5 Assembly of Air-Breathing Micro PEMFC

For Air-breathing Micro PEMFC, air is used as oxidant supply and driven by natural convection on cathode side, so the cathode side does not need any flow field plates. However, the acrylic plate should be designed to match the different shapes of current collector slices, as shown in Fig. 3.16. The acrylic plate and the assembly of the micro air-breathing PEMFC single cell are shown in Figs. 3.17 and 3.18, respectively. After the comparison between the forced convection and natural one, the representative one (9-circles) among these different shapes of current collector slice is chosen to make of a stack in series.

3.2.6 Assembly of Air-Breathing Micro PEMFC stack

In this study, 4-cells planner micro PEMFC stack is taken into investigation. The PDMS flow field plates used in these four cells are fabricated by the micro molding process just like the single cell. The cathode side of acrylic plate is also designed to match the shape of current collector slices. The acrylic plate, current collector slice, and the assembly of micro air-breathing PEMFC stack are shown respectively from Fig. 3.19 to Fig.3.23.

3.3 Test Station

A PEMFC test station, as shown in Figs. 3.24 and 3.25, is constructed to evaluate the characteristics of single or stack fuel cell. The components of test station are listed in Table 3.3.

Table 3.4 Instrument of Hardware Specifications

Hardware	***Number***	***Specification / Type***
Controlling Temperature System	5	25~90^{0}C T-type thermal couple
Heater	6	Humidify the gas: 250W Heating fuel cell: 50W Preheating pipe: 180W
Controlling Mass Flow Rate System	2	Hydrogen:0-400 sccm Oxygen: 0-2000 sccm
Display of mass flow rate	1	PROTEC PC-540
Valve of Back Pressure	2	250 psi Max
Back Pressure gauge	2	0~150 psi
Adding Humidity Container	2	Volume:1L Pressure:5Kgf/cm^2
Drain Valve	2	AW30-03BD
Switching Power Supply	2	3V,20A 24V,4.5A
Electromagnetic Valve	3	061317X 501062S
Hydrogen Detection	1	COSMOS 0-2000 ppm
19” Instrumental Frame	1	RA3570-0

Some parameters, such as flow rate, humidity and reheat temperature, can be adjusted in this station. After experiments, the

testing data, as listed in Table 3.4, can be collected by the software of test station.

Table 3.5 Function of Software

Item	***Function***
Automatic Control System	Controlling the Current, Voltage, Mass Flow Rate, Load
Testing Data	Current vs. Time, Voltage vs. Time, Power vs. Time, Tafel Data, Long-time Performance test

The limiting conditions of test station are listed in the Table 3.5.

Table 3.6 One or More PEMFC Testing Range

Type of electronic load	***PRODIGIT 3315D***
Current	0~15A
Voltage	0~60V
Power	75W Max

Fig. 3.16 shows the diagrams of components for the test station. Mainly, the system includes three parts, mass flow controllers, temperature controllers, and a DC electronic load.

3.4 Process of Fuel Cell Testing

In order to evaluate the performance of the micro PEMFC, the assembled cell is tested under the following process:

1. The inlets of the flow channel on both anode and cathode are plugged into the reactant supply tubes in the test station.
2. The current collectors are connected to the sensor on the test station to measure the voltage and current, and also connected to the load supply.
3. Adjust the flow rate of the reactant gas to the assigned value to let cell operate to obtain an open circuit voltage.
4. Apply load to let the cell discharge a current through the chemical reaction under an assigned voltage.
5. The current, voltage and power outputs from the cell can be recorded and plotted into the performance (I-V and I-P) curves.
6. Repeat the procedure for another load.

3.5 Uncertainty Analysis

Some form of analysis must be performed on all experimental data. The analysis may be a simple verbal appraisal of the results, or it may take the form of a complex theoretical analysis of the errors involved in the experiment and matching of the data with fundamental physical principles. Therefore, their accuracy should be confirmed before the analyses of experimental results. Experimental measuring must have errors, and experimental errors divide into the fixed (systematic) error and random (non-repeatability) error, respectively. Fixed error is produced after each experiments and it can be removed by proper

calibration and correction. However, Random error is different for every apparatus reading datum and hence cannot be removed. The objective of uncertainty analysis is to estimate the probable random error in experimental results.

3.5.1 Analyses of the Propagation of Uncertainty in Calculations

Uncertainty analysis estimates the uncertainty levels in the experiment. A method of estimating uncertainty in experimental results has been presented as follows:

Suppose a set of measurements is made and the uncertainty in each measurement may be expressed with the same odds. These measurements are then used to calculate some desired results of the experiments. The result R is a given function of the independent variables x1, x2, x3… xn. Thus,

$$R = R(x_1, x_2, x_3, \dots, x_n) \tag{3-1}$$

An individual xn, which affects error of R, can be estimated by the deviation of a function. A variation,δX_n, in xn would cause R to vary according to

$$\delta R_n = \frac{\partial R}{\partial x_n}\delta x_n \tag{3-2}$$

Normalize above equation by dividing R to obtain

$$\delta\frac{R_n}{R} = \frac{1}{R}\frac{\partial R}{\partial x_n}\delta x_n = \frac{x_n}{R}\frac{\partial R}{\partial x_n}\frac{\delta x_n}{x_n} \tag{3-3}$$

Equation (3-3) can be used to estimate the uncertainty interval in the result due to the variation in xn. Substitute the uncertainty interval for xn,

$$u_R = \frac{x_n}{R}\frac{\partial R}{\partial x_n}ux_n \tag{3-4}$$

To estimate the uncertainty in R due to the combined effects of

uncertainty intervals in all the xi, it can be shown that the best representation for the uncertainty interval of the result is

$$u_r = \pm\left[\left(\frac{x_1}{R}\frac{\partial R}{\partial x_1}u_1\right)^2 + \left(\frac{x_2}{R}\frac{\partial R}{\partial x_2}u_2\right)^2 + \cdots + \left(\frac{x_n}{R}\frac{\partial R}{\partial x_n}u_n\right)^2\right]^{\frac{1}{2}} \quad (3\text{-}5)$$

3.5.2 The Uncertainty of Test Station Apparatus

The apparatus must to be corrected by other standard instruments to make sure that they can normally operate and let the inaccuracy of the experimental results reduce to the minimum.

3.5.2.1 The Uncertainty of HP 6060B Electronic Load: u_v,u_A

The HP 6060B electronic load in the test station has been corrected its potential and current meter before experiment. The research uses FLUKE 8060A Digital Multimeter and Chroma Smart N300-040 Electronic Load to correct HP load box. Table 3.6 shows the error for different potentials.

Table 3.7 Uncertainty of Electronic Load Potential Meter

Standard value (V)	*Digital meter (V)*	*Uncertainty (%)*
20.00	19.81	-0.95
9.95	9.85	-1.00
8.02	7.95	-0.87
6.04	5.95	-0.99
5.00	4.97	-0.60
3.03	3.00	-0.99
1.00	0.998	-0.50
0.00	0.00	0.00

Next, the DC current meter of HP load box is corrected. They use

Chroma Smart electronic load and FLUKE digital meter to find the impedance of the shunt. They connect the shunt between HP load box and DC power source after correcting and adjust different potentials of power source, therefore, it can change the measurement current of load box meter. At the same time, the shunt measures a signal of current. After converting this signal, it can define the actual current of this circuit. Table 3.7 shows the error for different current.

Table 3.8 Uncertainty of Electronic Load Current Meter

Fluke digital meter (mV)	***Electronic load (A)***	***Conversion value ($\bar{A}$)***	***Uncertainty (%)***
0.00	0.00	0.00	0.00
1.69	1.00	1.02	1.96
5.05	3.00	3.04	1.32
8.37	5.00	5.03	0.60
16.71	10.00	10.05	0.50
25.04	15.00	15.06	0.40
33.41	20.00	20.09	0.45
50.21	30.00	30.19	0.63

3.5.2.2 The Uncertainty of Mass Flow Controller

In this study, there have three MFCs in the test station including anode, cathode and oxygen bleeding flow meter. The specified error is shown as follows:

$$\mathrm{ERROR}(\%) = \frac{\mathrm{CALAUATED} - \mathrm{TARGET}}{\mathrm{FULLSCALE}} \times 100\%$$

The ranges of MFC specified accuracy are 1000±5% with anode MFC, 2000±5% with cathode MFC and 500±1% with air bleeding MFC. They use the same company instrument, series 5850 MFC, as the

standard correction apparatus to correct these MFCs. The results are listed in the Table 3.8, 3.9, and 3.10, respectively.

Table 3.9 Uncertainty of Anode MFC

Standard value (sccm)	***Brooks MFC read value (sccm)***	***Measure value (sccm)***	***Uncertainty (%)***
1000	1002	1001	-0.10
500	501	499.8	-0.23
250	250.2	249.7	-0.23
0	0	0	0

Table 3.10 Uncertainty of Cathode MFC

Standard value (sccm)	***Brooks MFC read value (sccm)***	***Measure value (sccm)***	***Uncertainty (%)***
2000	1999.8	1999.4	-0.02
1250	1255	1253	-0.15
1000	1000.3	1000.2	-0.01
500	500.2	500	-0.03
0	0	0	0

Table 3.11 Uncertainty of Air Bleeding MFC

Output Voltage	***Brooks MFC read value (sccm)***	***Measure value (sccm)***	***Uncertainty (%)***
5	500	500.34	0.07
3.75	375	374.54	-0.09
2.5	250	250.32	0.06
1.25	125	124.54	-0.09
-0.001	0.0	0	0

They are anode, cathode and air bleeding flow meter, respectively. In these tables, the standard value means the setting flow rate, the Brooks MFC read value means the test station MFC readout value, the measurement value is the actual measured value. Then, these data can define the errors in different flow rates.

3.5.2.3 The Uncertainty of Temperature Controller

There are three temperature controllers in the test station. They are anode, cathode humidifier and fuel cell, respectively. The results of analyses are listed in Table 3.11, 3.12, and 3.13, respectively. In these tables, standard value means the setting temperature and the measure value means actual value, measured by the correction apparatus.

Table 3.12 Uncertainty of Anode Temperature Controller

Standard value (℃)	***Measure value (℃)***	***Uncertainty (%)***
25	25	0
35	35	0
50	50	0
70	70	0
85	84	-1.17
95	94	-1.05
100	99	-1

Table 3.13 Uncertainty of Cathode Temperature Controller

Standard value (℃)	***Measure value (℃)***	***Uncertainty (%)***
25	25	0
35	35	0
50	50	0
70	70	0
85	85	0
95	94	-1.05
100	99	-1

Table 3.14 Uncertainty of Cell Temperature Controller

Standard value (℃)	***Measure value (℃)***	***Uncertainty (%)***
25	25	0
35	35	0
50	50	0
70	70	0
85	85	0
95	95	0
100	100	0

3.5.3 The Uncertainty of Fuel Cell Power Density

The uncertainty of fuel cell power density comes from measuring process of fuel cell apparatus, therefore, the minimum scale of measuring voltage in the apparatus is 1mV, and the minimum scale of measuring current in the apparatus is 0.1mA. Appendix A shows the measuring uncertainty calculating process. Table 3.14 shows the uncertainty power density of PEMFC and micro PEMFC.

Table 3.15 The Measuring Uncertainty of Fuel Cell

PEMFC	The measuring uncertainty	Voltage	±0.10%
		Current	±0.02%
		Power	±0.10%
Micro PEMFC	The measuring uncertainty	Voltage	±0.10%
		Current	±0.01%
		Power	±0.10%

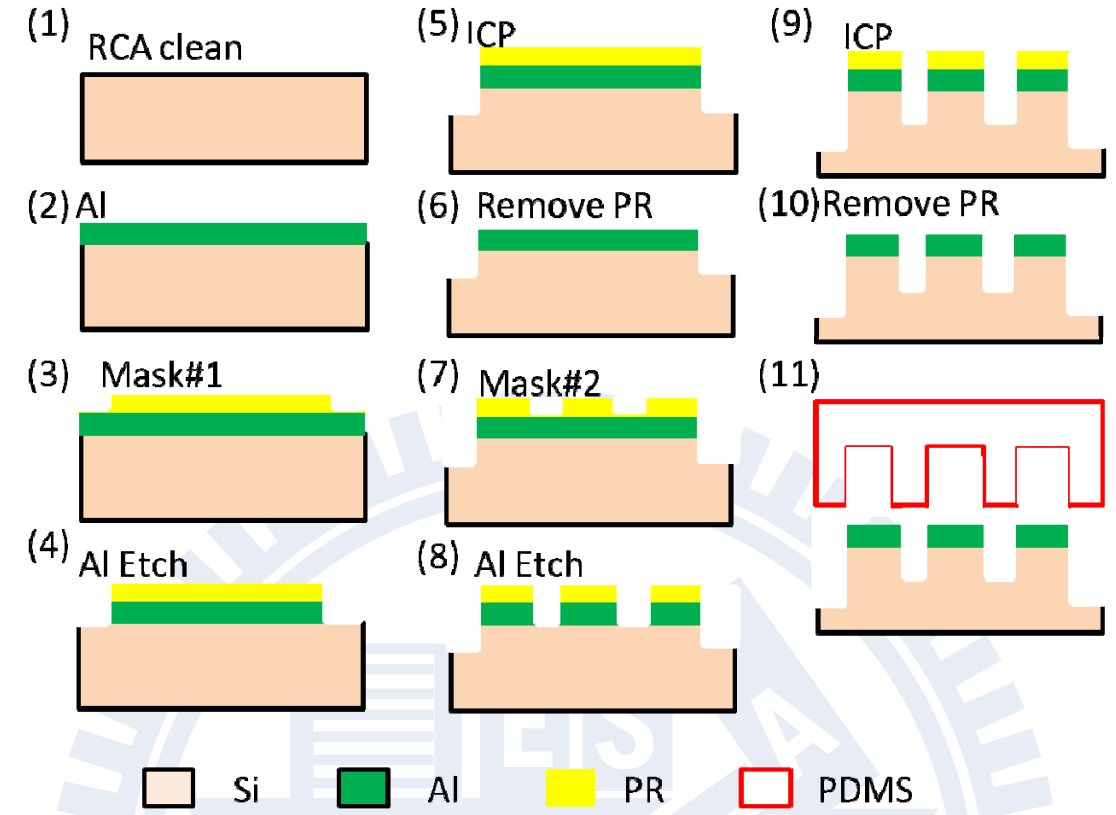

Fig. 3.1 Flow Charts of Flow Field Plate Fabrication

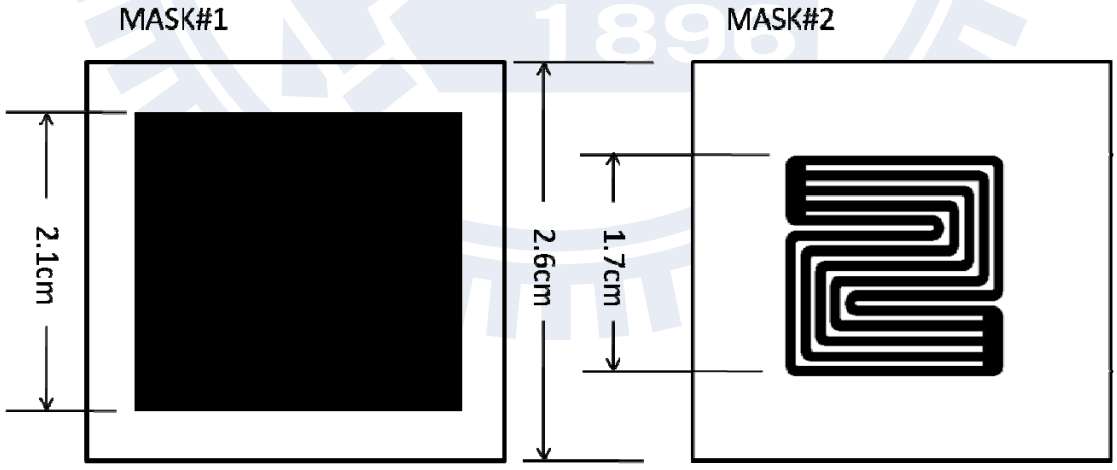

Fig. 3.2 Mask Design of Flow Field Plate Mold

Fig. 3.3 Wet Bench

Fig. 3.4 Spin Drying

Fig. 3.5 Sputter

Fig. 3.6 Track MK-8

Fig. 3.7 ICP

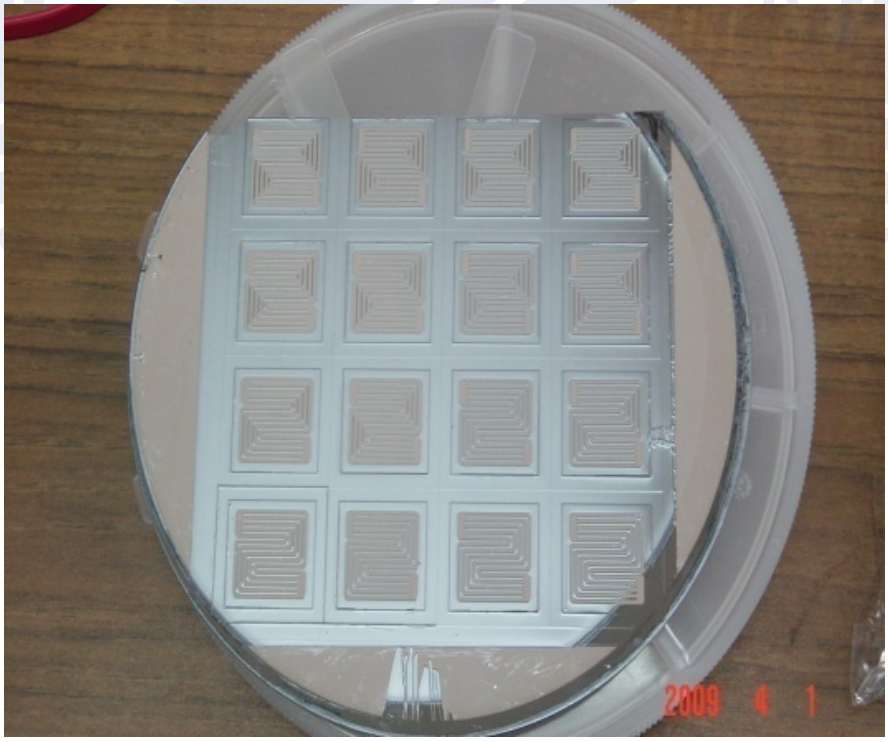

Fig. 3.8 Flow Field Plates Mold on the Silicon Wafer

Fig. 3.9 Vacuum Chamber

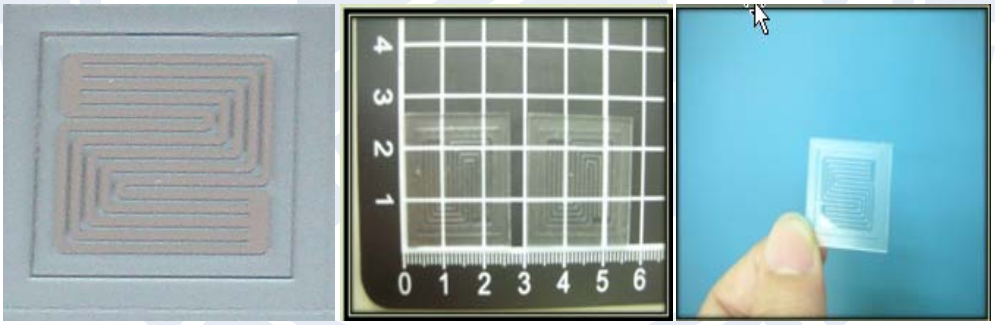

Fig. 3.10 Single Silicon Flow Field Mold and PDMS Flow Field Plate

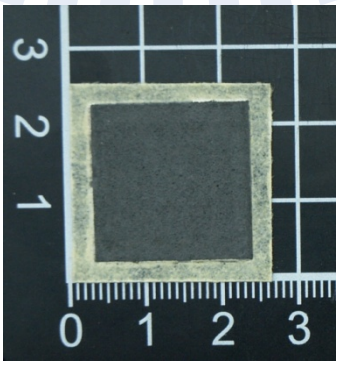

Fig. 3.11 GDL and MEA

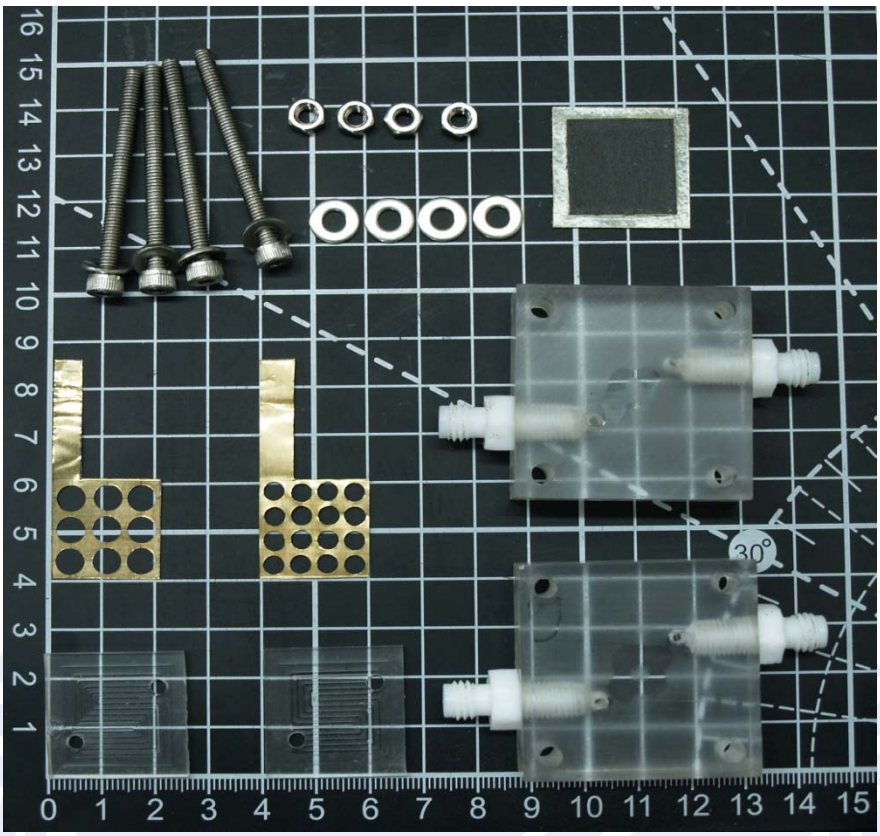

Fig. 3.12 Components of a Single Micro Fuel Cell

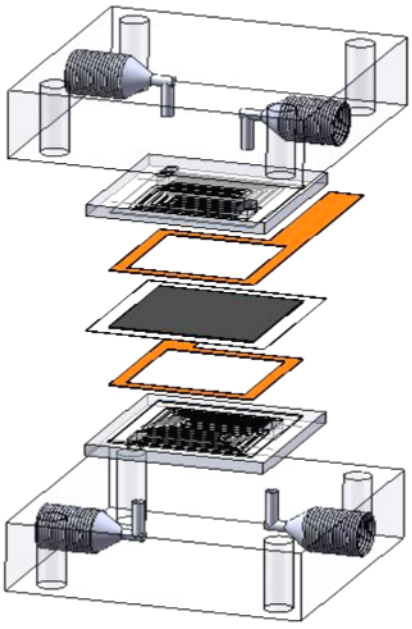

Fig. 3.13 Assembly of Micro PEMFC

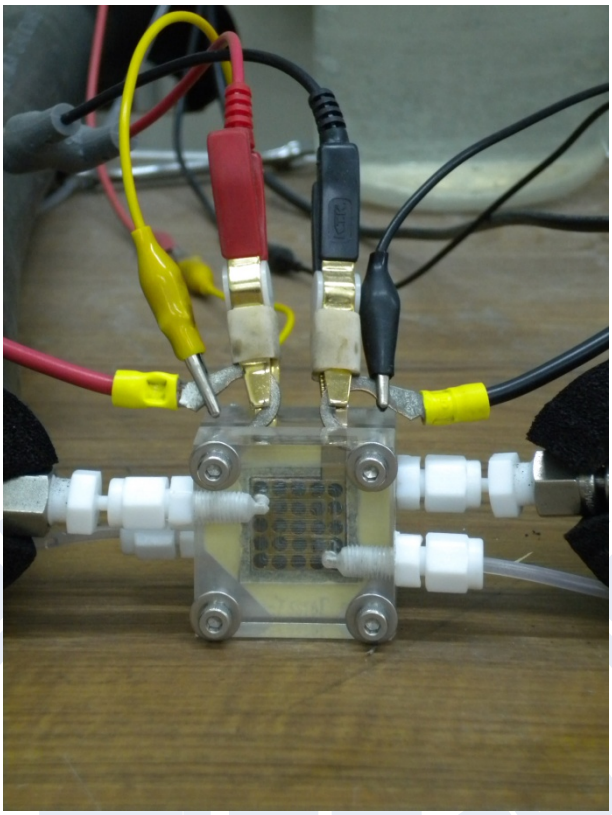

Fig. 3.14 Test of a Single Micro PEMFC

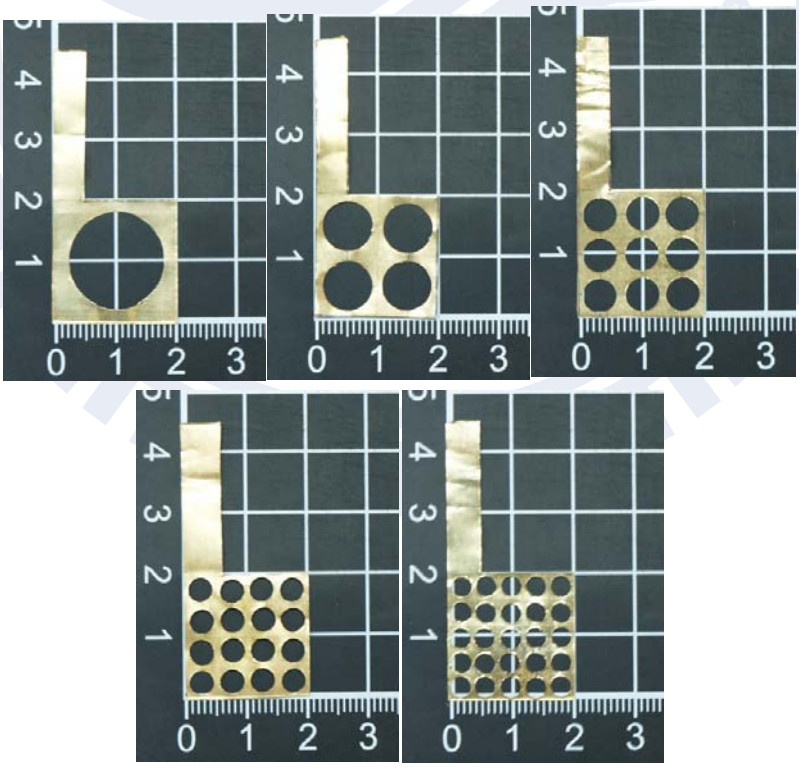

Fig. 3.15 Different Shapes of Current Collector Slice

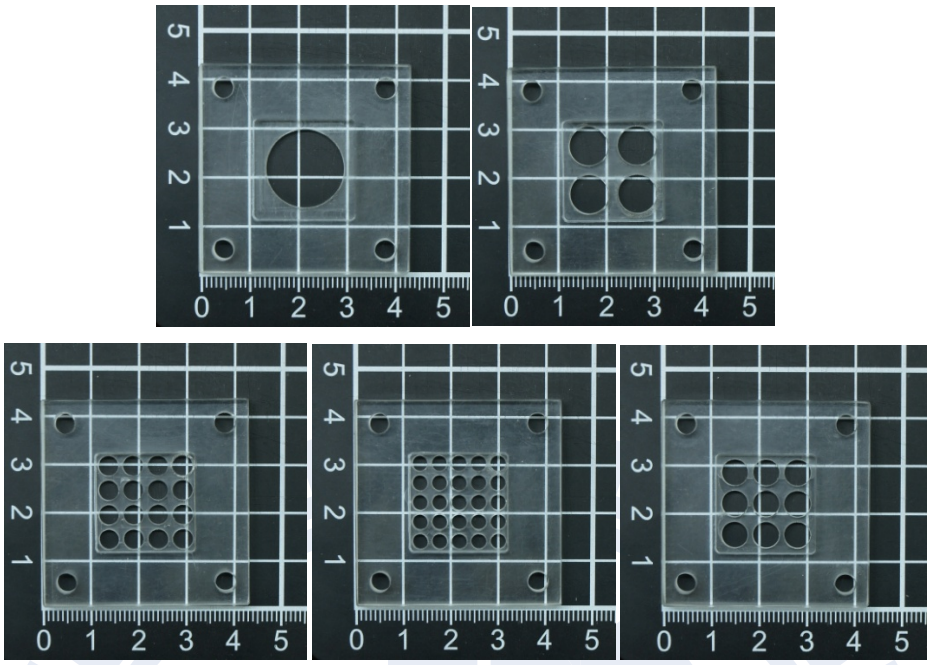

Fig. 3.16 Different Shapes of Acrylic Plate

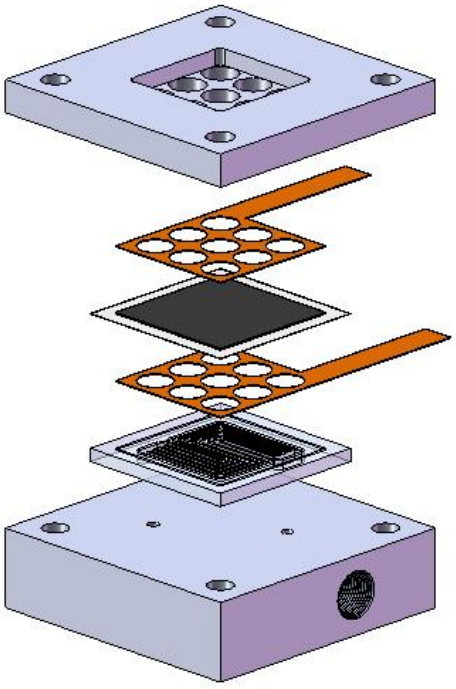

Fig. 3.17 Assembly of the Micro Air-breathing PEMFC Single Cell

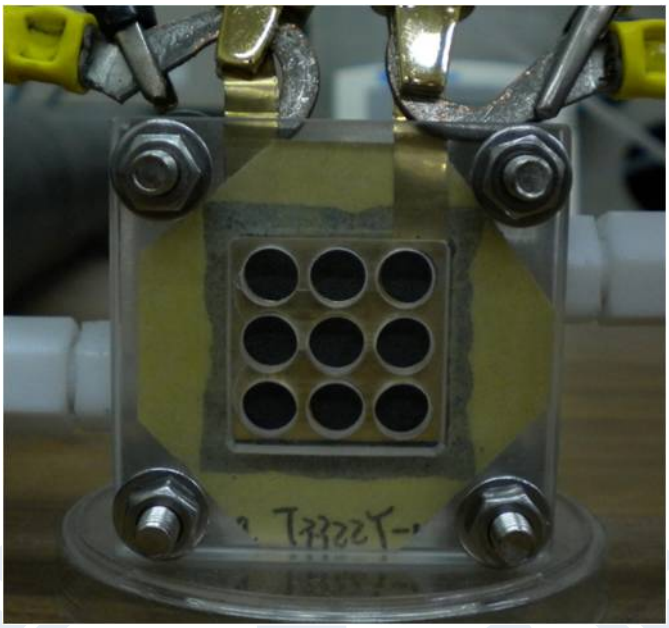

Fig. 3.18 Test of a Single Micro Air-breathing PEMFC

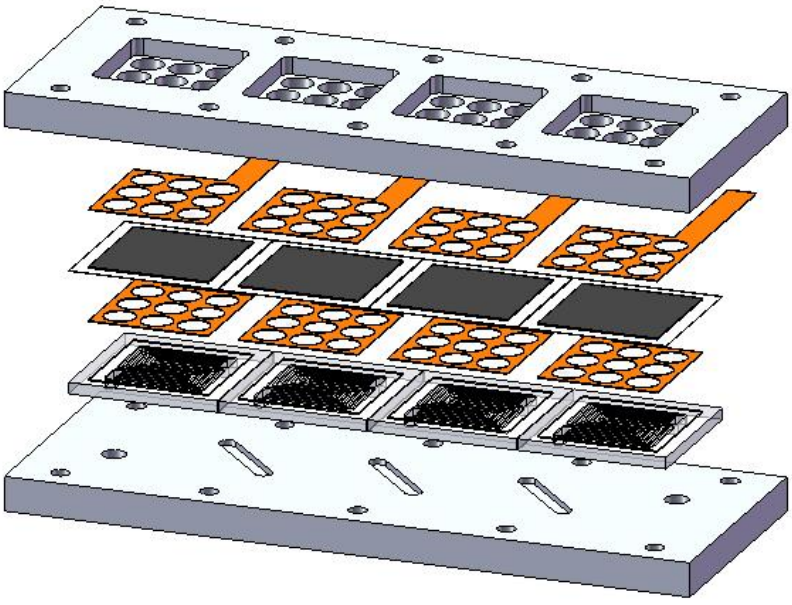

Fig. 3.19 Assembly of the Planar Micro PEMFC Stack

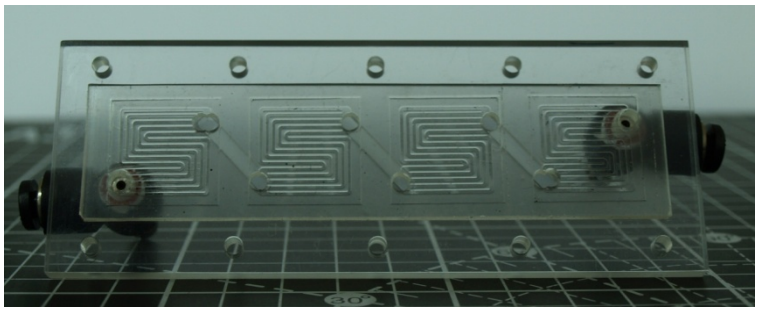

Fig. 3.20 Acrylic Plate and PDMS Flow Field Plate of the PEMFC Stack

Fig. 3.21 Anode Side of the PEMFC Stack

Fig. 3.22 Cathode Side of the PEMFC Stack

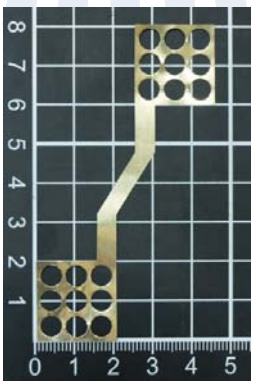

Fig. 3.23 Current Collector Slice of the PEMFC Stack

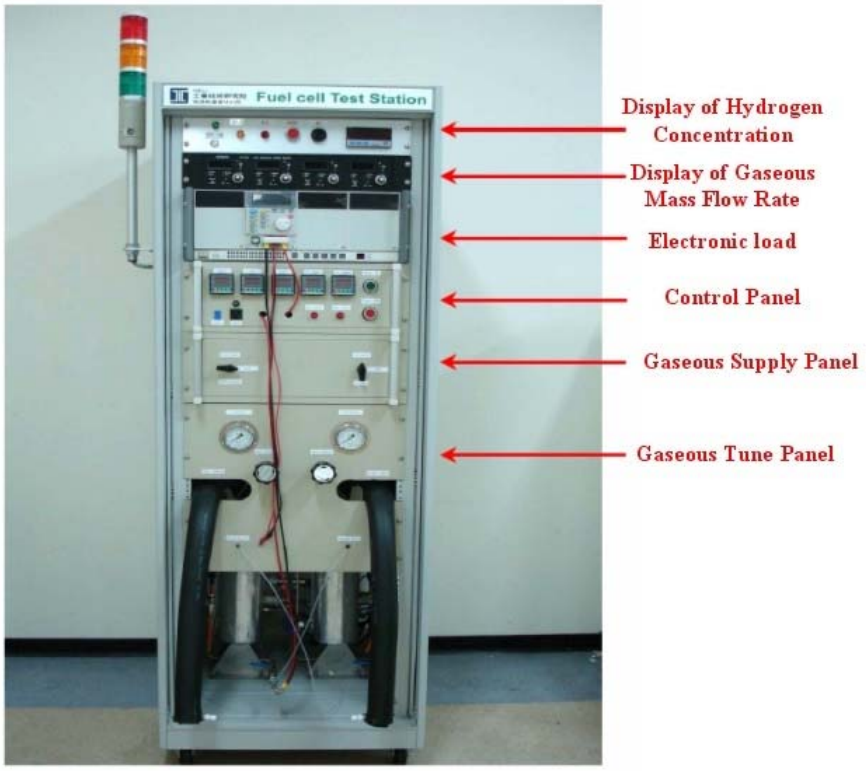

Fig. 3.24 Test Station

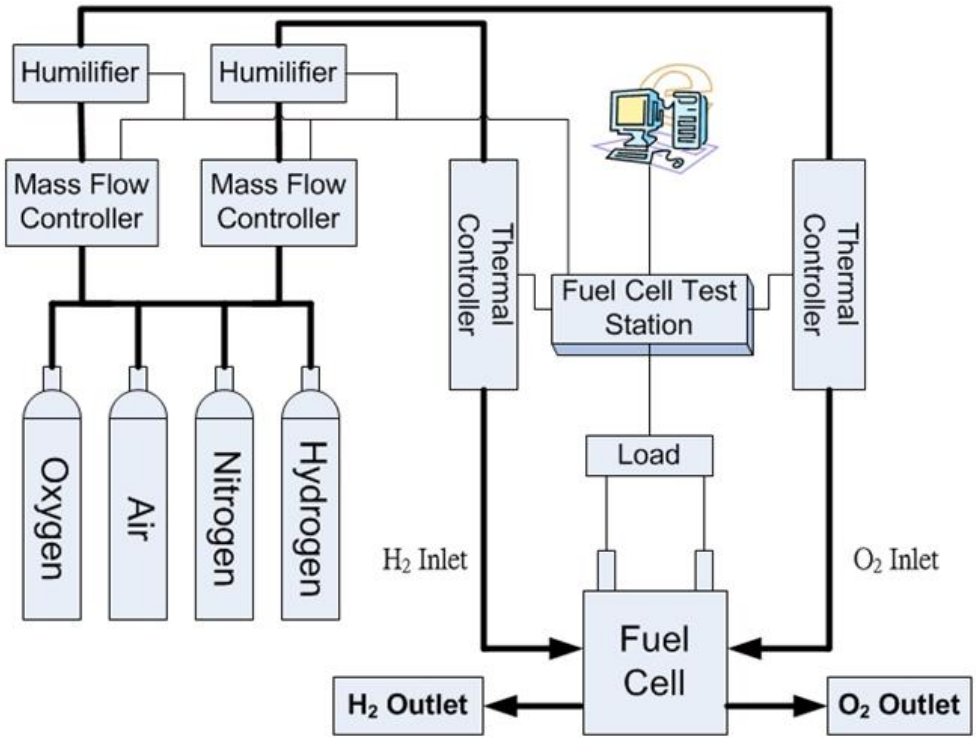

Fig. 3.25 Components of Test Station

Chapter 4

Results and Discussion

This study is divided into three parts. The research flow chart was already shown in Fig. 1.7. Firstly, a series of performance experiments on a single micro PDMS PEMFC was carried out and demonstrated in section 4.1. The experimental parameters included current collector shape, convection type and clamping force, respectively. Secondly, a planar PEMFC stack was designed and assembled to test the performance that is shown in section 4.2. The experimental parameters consisted of clamping force and fuel supply condition. In addition, in order to see the durability of continuous usage, both the single cell and the stack were tested for 14 hours at a fixed operating voltage. Finally, section 4.3 makes a comparison between PDMS-based PEMFC and silicon-based one to see the feasibility of micro PEMFC, which fabricated by using PDMS as the material of the flow field plate, and using the new design that combines both the gasket and flow field on the same plate.

4.1 Single Micro PDMS PEMFC

The followings are a series of performance experiments for the micro PDMS PEMFC.

4.1.1 Reference Case

Since a series of parametric studies was carried out, a reference case, served as the comparison base, was chosen in advance. Table 4.1 lists the testing conditions for the reference case of the single micro PEMFC. Note that the oxygen supplied from air in cathode was by means of

air-breathing and the temperature and humidity were kept in room environment condition because it is more convenient for future application. In air-breathing way, air enters cell by diffusing from the environment to the membrane through the holes on the current collector, so there is no need for another driving force to supply air in cathode.

Besides, the open ratio of flow field plates is defined as the ratio of the channel area to the total flow field plate area. In this study, 75% flow field plate ratio was applied since it had the best performance in Cheng's study [1]. Gas back pressure was kept 0 kPa on anode, implying that it was atmospheric pressure in the outlet of the fuel channel. The open ratio of Current collector slices is defined as the ratio of the sum of the open circle area to the total current collector area (see Figure 3.15). Convection type is divided into forced convection and natural one. The former has flow field plate in cathode, whereas the later let the cell breath air from the environment without flow field plate. Clamping force is the bolt torque applied on the cell, which decides the contact pressure between GDL and current collector, and the deformation of the flow field plate structure.

Table 4.1 Testing Conditions of Reference case

Reactant gases	
Anode	H_2 (99.9%)
Cathode	Air
Flow Rates	
Anode	H_2:20sccm (Forced convection)
Cathode	Air-breathing (Natural convection)
Gas Backpressure (Gauge)	
Anode	0 kPa
Temperatures	
Gas temperature	Room Temperature (25℃)
humidity	Room Condition (40%)
Open Ratio of Flow Field Plates (Channel / Rib)	
Anode Open Ratio	75%
Cathode Open Ratio	75%
Current Collector (thickness = 0.05mm)	
Material	Cu/Au
Shape	9-circle
Open Ratio	50%
Clamping Force	
0.5Kgf · cm	

The resultant performance curves (I-V, I-P and I-R) for reference case are shown in Fig. 4.1. Each experimental point was taken from the average of three measurements, and the corresponding error is less than 1%. There exist three major types of fuel cell losses, already mentioned in Sec. 2.2.2, therefore, the current density (I) increases with decreasing operating voltage (V) in I-V curve. From the figure it can be seen that the open circuit voltage (OCV) of I-V curve is only 0.946V instead of the ideal one, 1.23V due to activation losses. In the operating voltage range from 0.75 to 0.946V, the cell's voltage drops sharply because the

temperature and humidity of fuel cell do not reach balance conditions. As the stable conditions are achieved, the decreasing rate of voltage with increasing current density is slowed down. The decrease of operating voltage from 0.45 to 0.75V with current density is mainly influenced by the ohmic losses, which are influenced by not only the current collector shape and clamping force, but also the humidity of the membrane, determined by convection types. At the end of the I-V curve, however, the decreasing rate of operating voltage drops significant again because of the shortage of the fuel diffusion. At the limiting point, the power density is 99.6mW/cm2 and the corresponding current density is 340mA/cm2 at the voltage of 0.3V

I-P (current density-power) curve increases from zero at the beginning up to a maximum (regarded as the best performance), at which P = 129.775mW/cm2, I =285.225mA/cm2, and V= 0.45V, then, it drop sharply. The decrease in the power density is because it is constrained by the concentration losses due to a shortage of fuel diffusion, mentioned previously. However, the better operation voltage range is found from 0.5 to 0.7 V in this work but not at 0.45V exactly, because in such range it can prevent the cell from unstable operation caused by the high power density.

The current density-resistance curves (I-R) for reference case is also shown in Fig 4.1. The resistance is measured by the digital AC mΩ meter, which can detect the impedance during the ion transporting in the electrolyte and the resistance caused by the contact of the electrode at a fixed high frequency of 1kHz. Both the electrically conductive electrodes and the ion conductive electrolyte contribute to the resistance. It can be

seen that at low current density, the water produced during electrical chemical reaction is not enough to make the membrane approaching the saturated state, so the resistance is higher and becomes more unstable ($I < 100mA/cm^2$). At high current density region ($I > 100mA/cm^2$), the membrane contends more water and the resistance gradually reaches the stable state. The limiting resistance value in I-R curve is $0.0882ohm \cdot cm^2$ with the corresponding current density $340mA/cm^2$ at the voltage of 0.3V.

The resistance measured by the digital AC mΩ meter is different from the ratio of voltage to current (V/I, where V is the discharge voltage and I the current), representing the total resistance of whole loop in the cell. Both are shown together in Fig. 4.2 for comparison. The latter one (obtained by V/I calculations) is much greater than the former (measured) one. However, the difference gradually becomes smaller as the current density is greater, indicating that the impedance during the ion transporting in the electrolyte and the resistance caused by the contact of the electrode play more important role. Both are almost coincident at the limiting current density of $340mA/cm^2$.

The following parametric studies are focusing on the analyses for the effects of current collector shape, convection type, and clamping force on the performance of single micro PDMS PEMFC.

4.1.2 Effect of Current Collector Shape

In this part, 5 current collector shapes under the same open ratio of 50% were designed, which are 1-circle, 4-circle, 9-circle, 16- circle, and 25-circle, as shown in Fig. 3.15. Unlike the hydrogen in anode flowing through the channel on the flow field plate, in the air-breathing cell, air in

cathode has to diffuse from the environment into the cell by itself without any flow field plate. And then the air diffuse further to the membrane through the holes on the current collector, releasing electrons from the GDL to the current collector, and meanwhile forming water on the membrane.

As shown in Figs. 4.3 and 4.4, which are I-V and corresponding I-P curves under different current collector shapes, even under the same open ratio, the performance increases with an increase of the circle numbers from one to twenty-five. That means the better reactions and more electrons are achieved for the cell having more holes on the current collector. Two possible reasons contribute to this result: one is that the average distance the electrons have to pass from the GDL to the current collector becomes shorter; the other is that the non-open area blocking the fuel diffusion becomes smaller; see Fig. 4.5.

When the chemical reaction is processing, electrons are not only produced on the area covered by the current collector, but also on the open area. If the electrons are produced on the open area, they have to pass through the GDL to the current collector, meaning that the path is with higher electric resistance such that lowers down the cell performance. Besides, the gas and water produced have to remove and transport by diffusion between the covered and uncovered area of current collector. If the covered part is too deep for the fuel to diffuse, the performance will also decrease because of the difficult diffusion.

However, the membrane would become more humidified if the water could not diffuse smoothly and be carried away by the gas, then the total cell resistance would be lowered. Therefore, from the I-R curve

shown in Fig. 4.6 it is found that, although the total cell resistance decreases from 1-circle one to 25-circles one, making the maximum current density increase more, the cell resistance of the 16-circle is smaller than that of the 25-circle one because of the better water diffusion effect.

Table 4.2 summarizes the experimental results of the peak power density, the increase ratio of peak power with respect to the one of reference case, and the maximum current density that each cell can be extended for five different current collectors for the air-breathing cell (Figures 4.3, 4.4 and 4.6). It can be seen that both the Peak Power Density and Max Current Density Extended at 0.3V increase with the increment of hole number on current collector. However, the peak power increase ratios in 16- and 25-circle cases are 4.3% and 11.5% comparing to that of reference case. Therefore, considering the factors among of structural strength, ease of manufacture, and increasing percentage of performance, this study proposes 9-circle current collector to be used in the present design for both air-breathing and forced convection cells. This is also the reason why this work selects the 9-circle current collector in the reference case.

Table 4.2 Experimental Results of Five Different Current Collector for Air-breathing Cell

Properties / Shape	Peak Power Density (mW/cm^2)	Peak Power Increase Ratio w.r.t. Reference Case	Max Current Density Extended at 0.3V (mA/cm^2)
1-circle	61.7	-52.4%	180
4-circle	97.0	-25.3%	284.6
9-circle	129.8	-	340
16-circle	135.3	4.3%	352
25-circle	144.7	11.5%	370.5

4.1.3 Effect of Convection Type

Different from the air-breathing cell, the air is supplied through the flow channel on cathode in the forced convection one. From Figures 4.7 and 4.8, which are I-V and the corresponding I-P curves under forced convection, it can be found that in the low current density region, the I-V curve of 25-circle is below those of 9-circle and 16-circle at $I < 162mA/cm^2$ and $I < 261\ mA/cm^2$, respectively that is different those in Fig. 4.2 for air-breathing cell. It is because forced convection tends to carry away the water and make the membrane dryer. Just as mentioned previously in air-breathing cell, the current collector with fewer holes can block more water from diffusing away between the current collector and GDL, so at lower current density region, where the electric chemical reaction is not too strong and produces less water, the membrane becomes dryer in 25-circle one that makes it perform worse than the other two. Behind those two critical current densities, the performance of 25-circle current collector becomes better because the reaction is stronger and membrane is wetter. Even though, the performance trend of the forced convection cell is quite similar to that of air-breathing single cell at high

current density region. So does the I-R curve as shown in Fig. 4.9. In other words, the qualitative difference in performance among these shapes of current collectors is not affected by the convection way. In addition, Figure 4.9 (I-R curves) shows that the cell resistance of the 16-circle is almost coincident with the one of 25-circle because of the humidify effect mentioned previously in the air-breathing cell.

Now, compare the quantitative difference between the air-breathing and forced convection cells by using the 9-circle current collector (see the reference case in Table 4.1). As shown in Figs. 4.10 (I-V curve) and 4.11 (I-P curve), there exist intersections (occurred at I = 200 mA/cm^2 approximately) on both I-V and I-P curves for these two types of cells. It is explained that although forced convection can enhance the air diffusion rate, it will accelerate the heat loss to lower down the temperature, which the electrochemical reaction needs. Besides, the water evaporation rate is simultaneously increased so that the water produced by electrochemical reaction is insufficient relatively. The combined effects of the temperature drop and higher water evaporation rate result in the resistance of electrochemical reaction and ion conductivity of membrane, causing the performance drop accordingly at lower current density region. Behind that (I > 200 mA/cm^2), concentration losses for forced convection cell is lower owning to the sufficient fuel diffusion rate helping to eliminate the concentration loss, resulting in a better performance than that of air-breathing cell.

From above discussion, it can conclude that forced convection cell is a better choice for long-time high current-density output; in contrast, air-breathing cell is more suitable for lower current density output.

4.1.4 Clamping Force Effect

4.1.4.1 Micro Air-breathing PDMS PEMFC

In this part, the clamping force effect on the performance of air-breathing cell is observed. The torque on each bolt on the cell (4 bolts total) was increasing from 0.5 to 3.0Kgf · cm. The results are shown in Figs. 4.12 (I-V curve) and 4.13(I-P curve). It can be seen that the performance of the cell has a significant improvement when the clamping torque of each bolt is raised from 0.5 to 1.0Kgf · cm, increases slowly from 1.0 to 2.5Kgf • cm, and starts to decrease after 3.0Kgf · cm. From the I-R curves shown in Fig. 4.14, however, the cell resistance is all decreased as the clamping torques rising from 0.5 to 3.0Kgf • cm.

Basically, the cell's performance is improved by the applied assembly pressure because of the reduction in the electrical contact resistance between the current collectors and the GDL. However, when the applied pressure is getting higher, the porosity of the GDL and the size of the fuel flow channel will be squeezed simultaneously, causing the resistance increase of the fuel diffusion. The total performance will not be improved if the resistance of fuel diffusion is too much to be compensated by the reduction of the electrical contact resistance. Therefore, an appropriate clamping torque should be considered carefully to enhance the performance without damaging the GDL and narrowing down the fuel flow channels. In the present study, a torque of 2.5 Kgf • cm is recommended

4.1.4.2 Comparison of PDMS- and Silicon-Base Cells

As mentioned in sec. 1.1, since the structure of silicon-based flow field plate is too weak to prevent the problem of crack while assembling, the largest clamping torque applied can only be 0.5Kgf · cm. Take PDMS- and Silicon-Base cells for comparison under the same clamping torque of 0.5Kgf · cm, whose results are shown in Fig. 4.15 (I-P and I-R curves). It is found that no matter in the power or the resistance exhibitions, the PDMS-based PEMFC performed much better than the Silicon-based one. Their reasons are as follows: First, silicon is not as elastic as PDMS so that it cannot make the perfect contact between the current collectors and the carbon fiber on the GDL, causing the higher resistance; Second, silicon's nonelastic property also produces the gas-leaking problem that lowers down the performance; Third, the non-opaque property of Silicon makes the assembly hard to be aligned precisely between constituting parts that may bring about more unpredictable problems. Owing to the elastic and transparent property, PDMS-base cell apparently is more suitable for the micro air-breathing PEMFC than the silicon-based one. It can also be seen from the I-R curve in Fig. 4.15 that the resistance of the PDMS-base cell is smaller than that of silicon-base cell. The reasons are similar to what just discussed above.

4.1.5 Durability Test of Single Micro PDMS PEMFC

To investigate whether the micro PDMS PEMFC performance is still able to be stable after the long-time test, the single micro PDMS PEMFC was tested for 14 hours continuously at different fixed operating voltages,

which are 0.7V, 0.6V, 0.5V and 0.4V, respectively.

Figure 4.16 shows the results at four different operating voltages, which are presented by power density as a function of time. In the first two hours, the four performance curves appear to have a little instability because the temperature, humidity and water management of fuel cell do not reach balance conditions yet; however, the system becomes stable obviously after the two hours. This result means that the single micro PDMS fuel cell can maintain a stable power output for a long time use up to 14 hours.

4.2 Micro Planar Air-breathing PEMFC Stack

In this part, a stack made of four micro PDMS planar air-breathing PEMFCs in series was designed; see Fig. 3.19, which used 10 bolts around four cells, and the 9-circles current collectors were adopted on both anode and cathode.

4.2.1 Effect of Clamping Force

Just like the single cell, increasing the clamping torque reduces the electric contact resistance and enhances the performance, but still there is limitation. In this experiment, the fuel flow rate was kept 60sccm in anode, and air-breathing was used in cathode. As shown in Figs. 4.17, 4.18 and 4.19, which are I-V, I-P and I-P curves, the range of the power increase is getting smaller as the applied torque becomes greater, implying that the assembly force cannot be over a certain limit, or the performance will not be further improved but damages of the GDL and flow channels can be possibly caused.

4.2.2 Effect of Fuel Supply condition

In this part, effects of two types of hydrogen supply conditions are studied. One is that the outlet is dead-end with a constant gage pressure of 0.5atm applied and kept at inlet; the other one is that both inlet and outlet are open with H2 supply volume flow rates of 60sccm and 120sccm, respectively. Dead-end means the outlet of the channels is closed that fuel must be used up within the cell. In this experiment, air-breathing was also used as the air supply in cathode, and the applied clamping torque was kept 1.5 Kgf · cm.

4.2.2.1 Effect on the Whole Stack

Figure 4.20 shows the I-V curves. For open outlet condition, it can be seen that, although all the I-V curves are almost coincident; however, the performance of 40sccm is better than those of 60 and 120sccm, especially in the larger current density range. Apparently, the air-breathing way cannot provide enough air into stack for the reactions of 60 and 120sccm of H_2 supply. Such oversupply of H_2 ($\geq$60 sccm) leads to a lower reaction, similar to the situation of fuel-rich combustion.

In dead-end condition, the performance at low current density is almost the same as that of the open outlet condition with a flow rate of 60sccm, and a litter lower than that of 40sccm, moreover, the limiting current density can be extended to a higher value (from I = 1103mA to I = 1209mA), implying that the concentration loss is significantly improved due to the reinforced complete reaction in that region.

Obviously, the increase of flow rate is not a best way to improve the concentration loss in this air-breathing stack experiment because of the

limited air supply.

4.2.2.2 Effect on Each Cell

Designate the cell connecting to hydrogen inlet as the first cell and the one to outlet as the forth cell. From I-V curves for each cell shown in Figs. 4. 21, 4.22 and 4.23 under different fuel supply conditions, it can be found that, no matter what kind of fuel supply condition, the third cell always has the best performance, and the second one is next, after that is the first one, and the forth has the worst performance. As expected, the forth cell has the worst performance because this flow field design cannot supply the enough fuel in time to avoid the serious concentration loss at the end. And the third cell, which has the best performance, is mainly affected by the temperature and humidity. When the fuel travels through the first cell to the third one, the temperature has already been reheat from room temperature to higher one. Similarly, the fuel has also been humidified a lot that lowers down the resistance. These two factors make the electric chemical reaction to be more favorable. Therefore, owing to the temperature and the concentration loss effects, each cell in the same stack has different performance under this design (in series arrangement).

4.2.3 Stack Durability Test

In the durability test of the micro planar PDMS PEMFC fuel cell stack (in series arrangement), it was tested at various fixed operating voltages which are 2.8V, 2.4V and 2.0V (averaged 0.7V, 0.6V, and 0.5V for each cell), respectively. The results are also presented by power density as a function of time in Fig. 4.24. Similar to the single cell durability test, in the first two hours, these thee stack performance curves

appear to have a little instability and the system becomes stable obviously after the two hours. These results mean that the stacks can maintain a stable power output for a long time use up to 14 hours approximately.

4.3 Comparison between Silicon Base and PDMS Base

4.3.1 Forced Oxygen Supply

To compare the performance between the silicon-based flow field plate and the PDMS-based one, one result in Cheng's study [1] was taken to make a comparison with the present one of PDMS under the same experimental parameters, listed on Table 4.3.

Table 4.3 Testing Conditions

Reactant Gases	
Anode / Cathode	H_2 (99.9%) / O_2
Flow Rates	
Anode / Cathode	H_2:30sccm / O_2: 30sccm
Gas Backpressure (gauge)	
Anode / Cathode	0 kPa / 0 kPa
Current Collector Slices	
Material	Cu/Au
Temperatures	
Gas reheat temperature	60℃
Gas humidified temperature	60℃
Open Ratio of Flow Field Plates	
Anode Open Ratio	75%
Cathode Open Ratio	75%

As mentioned previously, the present new design and fabrication method not only make assembly more convenient and mitigate the crack and gas-leakage problems, but also help the micro PEMFC planar stack more easily produced. Because the problems mentioned above are improved, it is not surprising that the PDMS-based one has a better

performance with a 24% of peak power more than that of the silicon-based one as shown in Fig. 4.25.

4.3.2 Air-breathing

Similar to last section, the air-breathing cell performance now is compared between Chang's and present works. The experimental parameters are listed in table 4.4.

Table 4.4 Testing Conditions of Case

Reactant Gases	
Anode	H_2 (99.9%)
Cathode	Air
Flow Rates	
Anode	H_2:30sccm (Forced convection)
Cathode	Air-breathing (Natural convection)
Gas Backpressure (gauge)	
Anode	0 kPa
Current Collector Slices	
Material	Cu/Au
Temperatures	
Gas reheat temperature	Room Temperature(25℃)
humidity	Room condition (40%)
Open Ratio of Flow Field Plates	
Anode Open Ratio	75%
Cathode Open Ratio	75%

Figure 4.26 is the I-P curves for both experimental studies according to the test conditions of Table 4.4. Similarly, the PDMS-based one has a better performance than that of the silicon-based one with 24.5% more in peak power. It also means that the new design and fabrication method of PDMS PEMFC can improve the performance even for the air-breathing is

the way of air supply.

4.3.3 Liquid Water Produced by Thermal Effect

To observe the phenomena of liquid water produced on the GDL and flow field plate, both silicon-base air-breathing cell and the PDMS-base one were taken apart after they were tested for 15 minutes at a fixed voltage of 0.5V with the parameters the same as those in sec 4.3.2. The pictures are shown in Fig. 4.27 and 4.28, respectively. It can be seen that there are some liquid water forming on the silicon-base cell's GDL and flow field plate, whereas no water is found on the PDMS-base cell's ones because trace-amount of water is evaporated quickly as soon as the cell is disassembled. The reason is that PDMS is a material with much lower heat conductivity than that of silicon, so it can prevent heat loss by conduction of the flow field plate during electric chemical reaction, and make the cell temperature rising quickly to effectively evaporate the liquid water into vapors, easily carried away by the gas flow.

The micro air-breathing PEMFC produces less heat than the non-micro one. If the heat is lost too much, then it will lower down the temperature further and make more water vapors condensed into liquid water, causing water flooding in the cell. In the future the micro air-breathing PEMFC is used in commercial goods, it is very important to avoid the water flooding problem that can possibly damage the 3C products. PDMS, with less water flooding effects, apparently is a better material than silicon for micro air-breathing fuel cell.

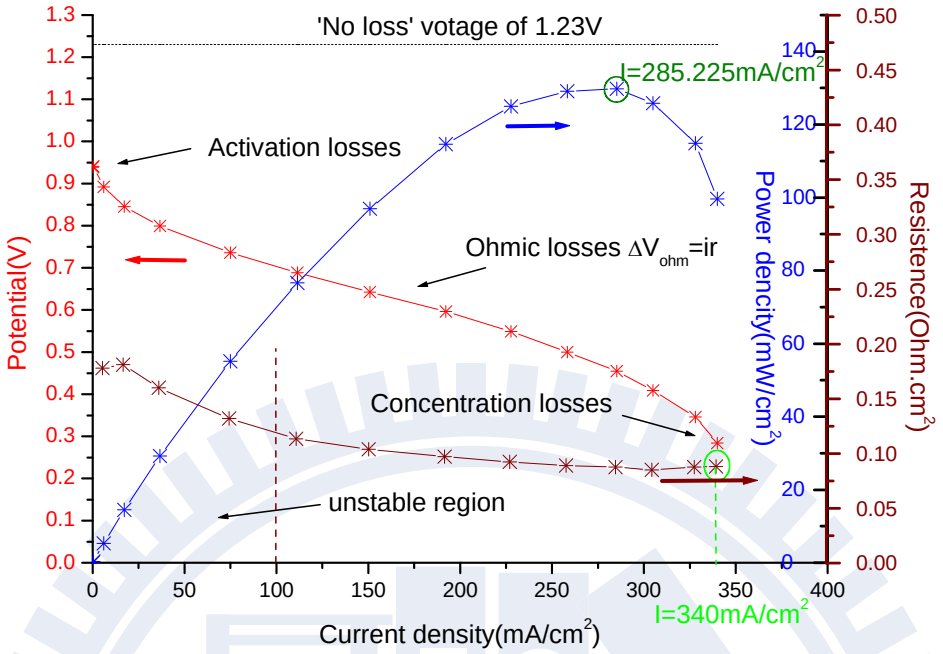

Fig. 4.1 Performance Curves (I-V, I-P and I-R) for Reference Case

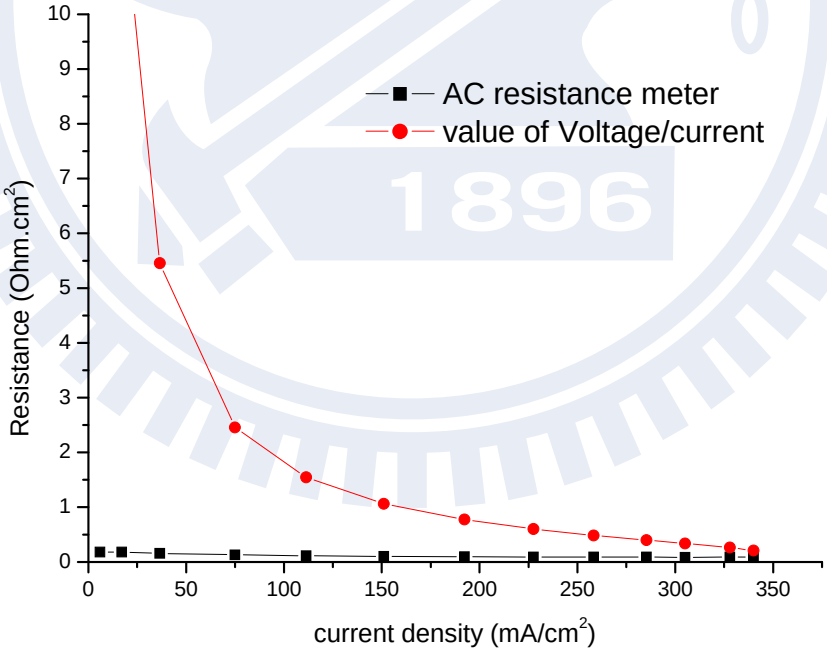

Fig. 4.2 Resistance Value from the Voltage Divided by the Current

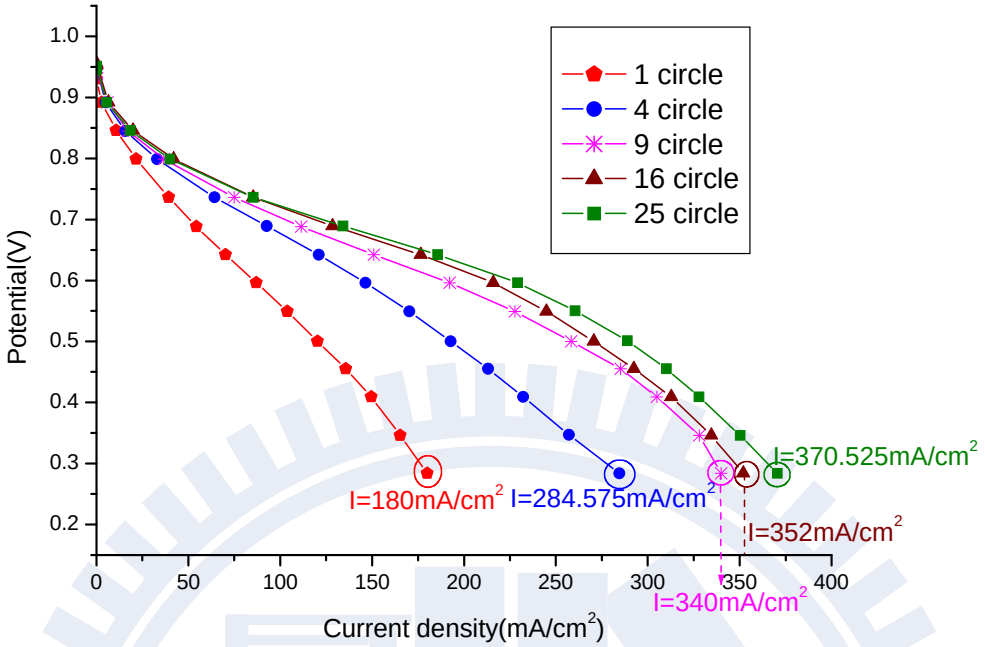

Fig. 4.3 I-V Curves of Five Different Current Collectors for An Air-breathing Cell

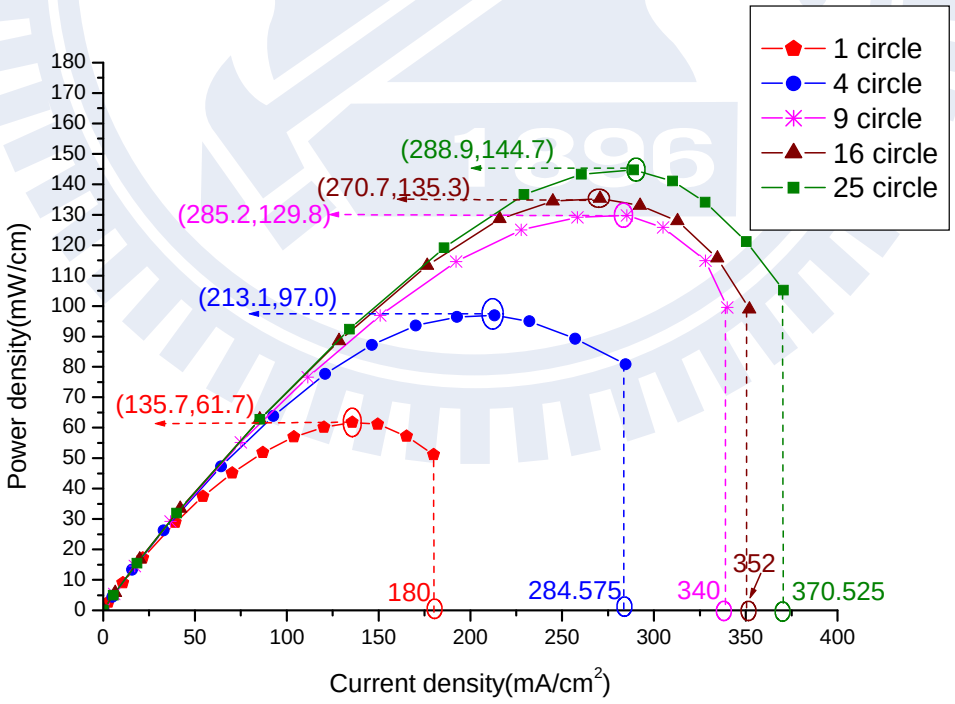

Fig. 4.4 I-P Curves of Five Different Current Collectors for An Air-breathing Cell

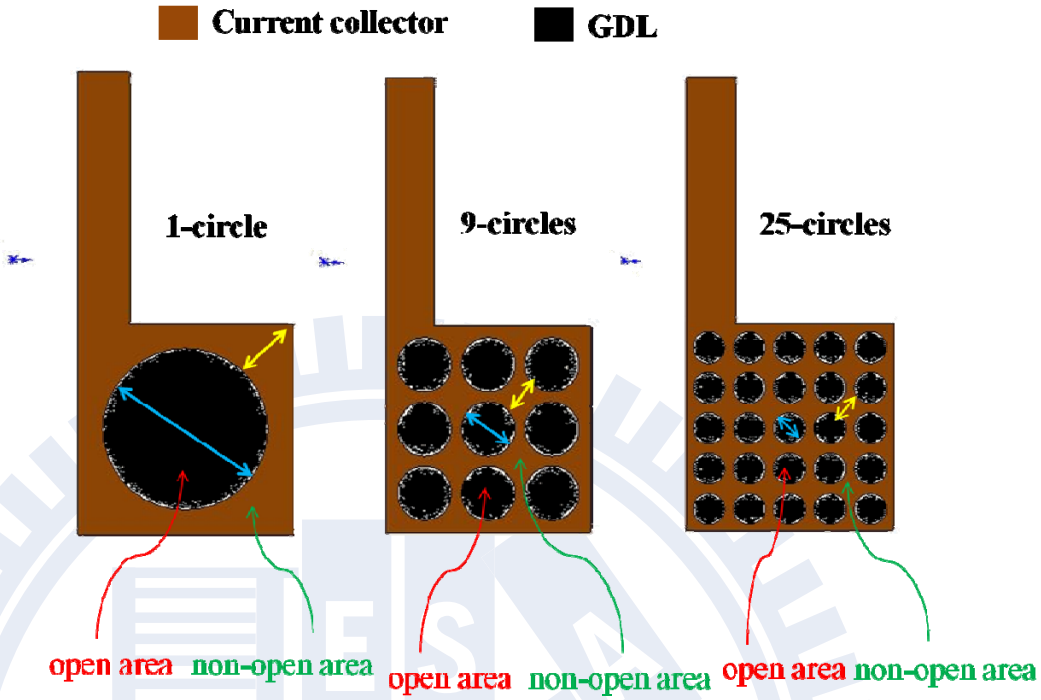

Fig. 4.5 Comparison of Average Distance of Open Area and Non-open Area among Difference Current Collectors

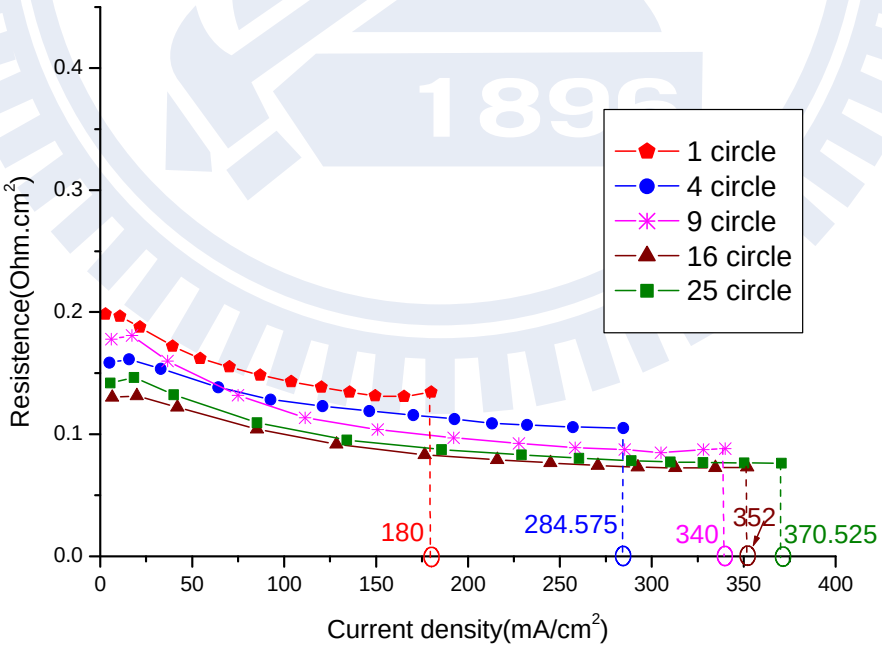

Fig. 4.6 I-R Curves of Five Different Current Collectors for An Air-breathing Cell

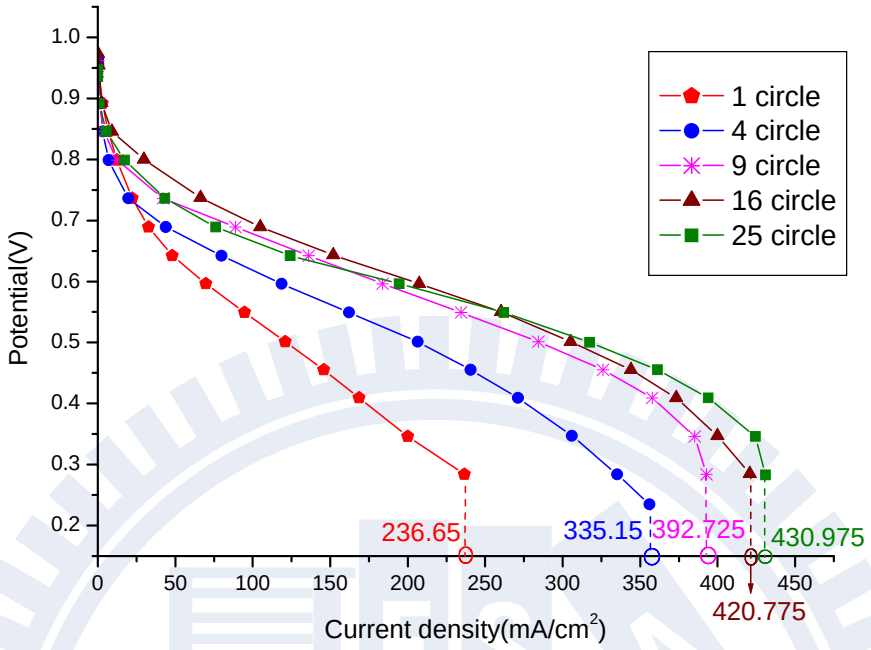

Fig. 4.7 I-V Curves of Five Different Current Collectors under Forced Convection

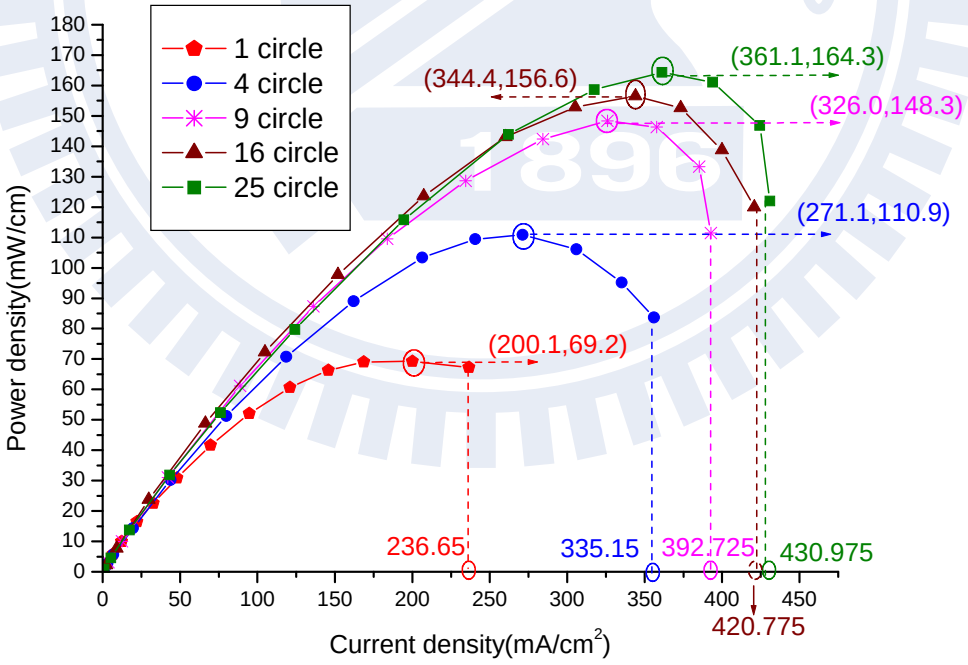

Fig. 4.8 I-P Curves of Five Different Current Collectors under Forced Convection

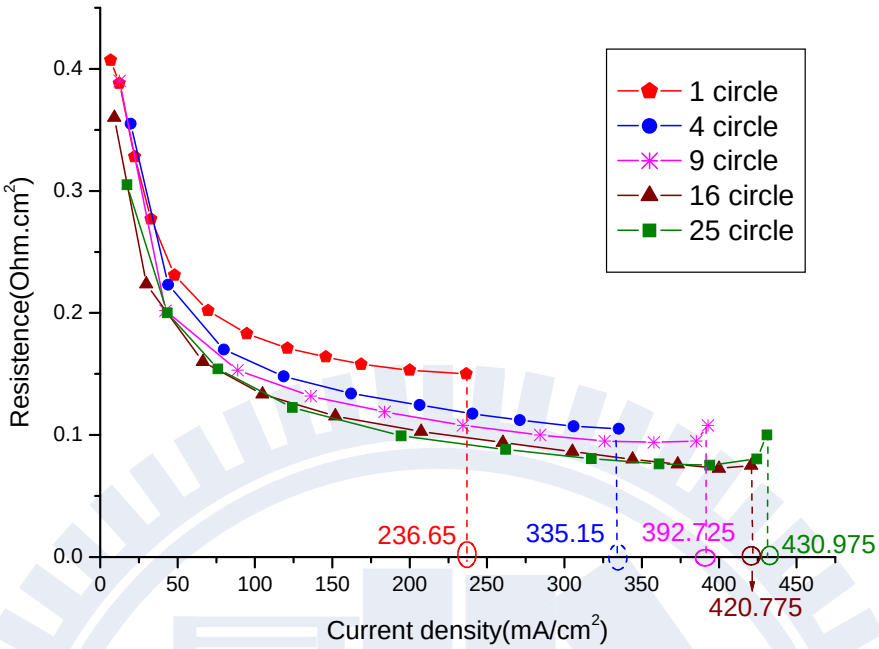

Fig. 4.9 I-R Curves of Five Different Current Collectors under Forced Convection

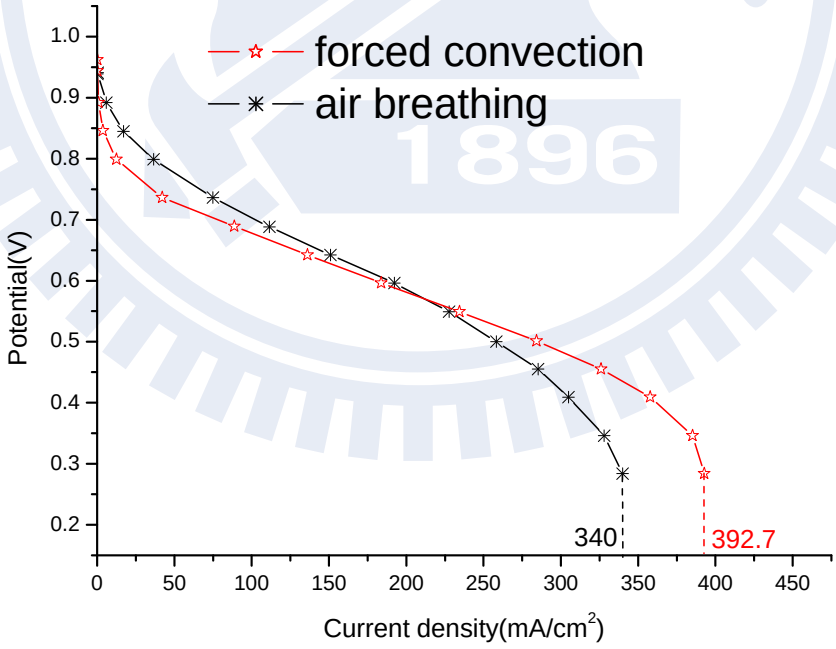

Fig. 4.10 I-V Comparison of Forced and Natural Convection Effect

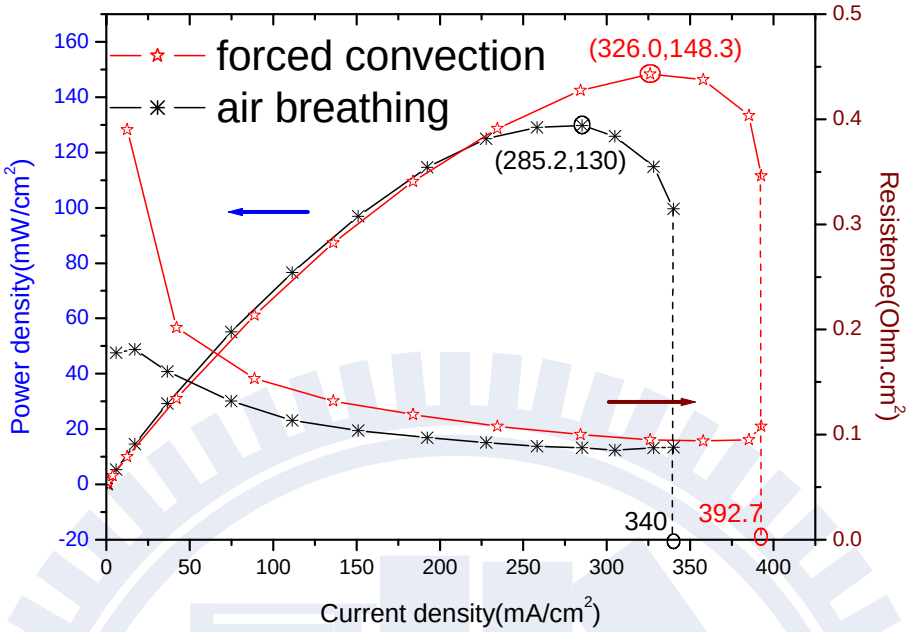

Fig. 4.11 I-P and I-R Comparison of Forced and Natural Convection Effect

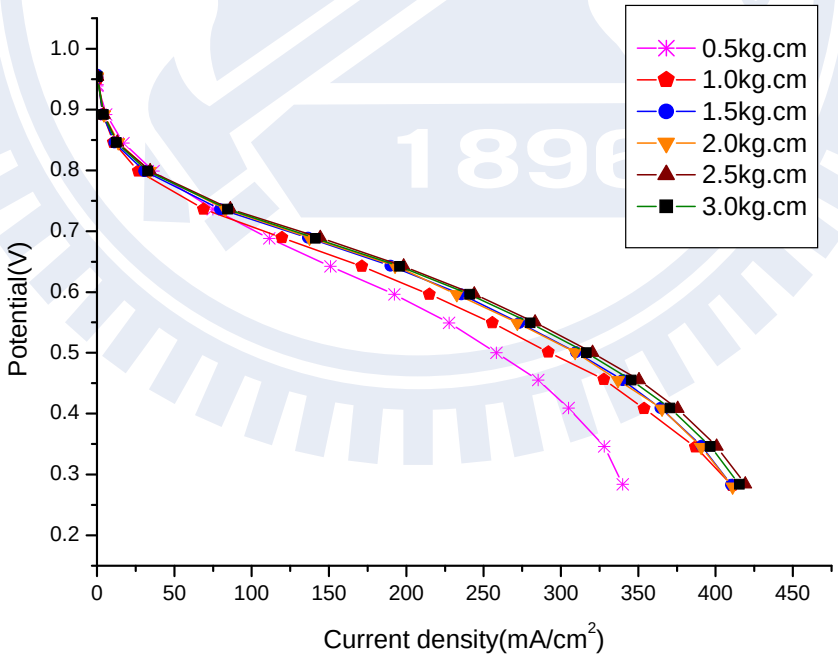

Fig. 4.12 I-V Curves of Clamping Fore Effect on Single Cell

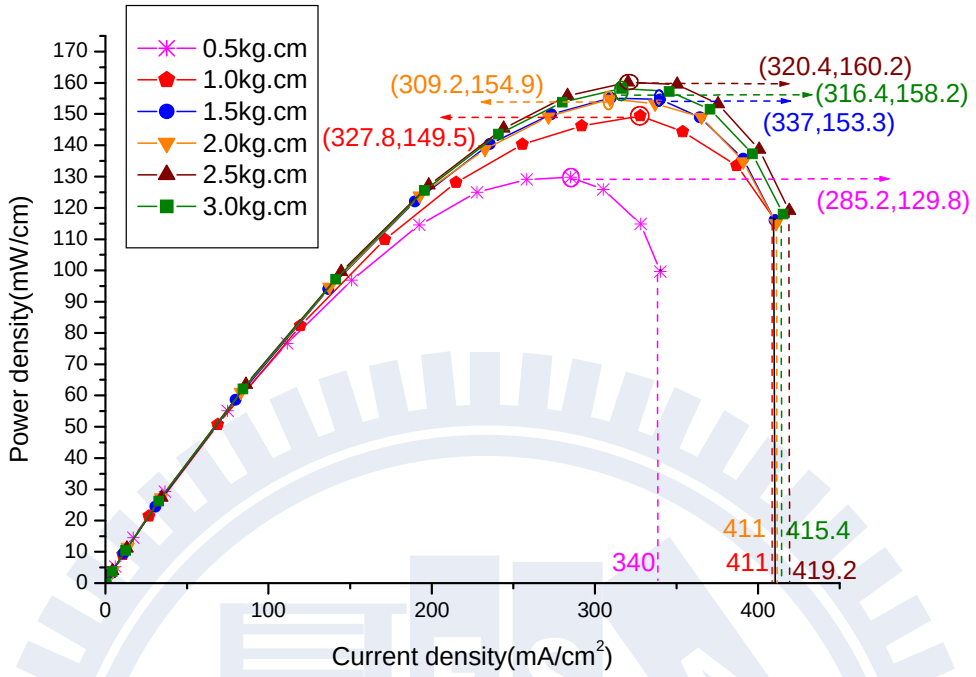

Fig. 4.13 I-P Curves of Clamping Fore Effect on Single Cell

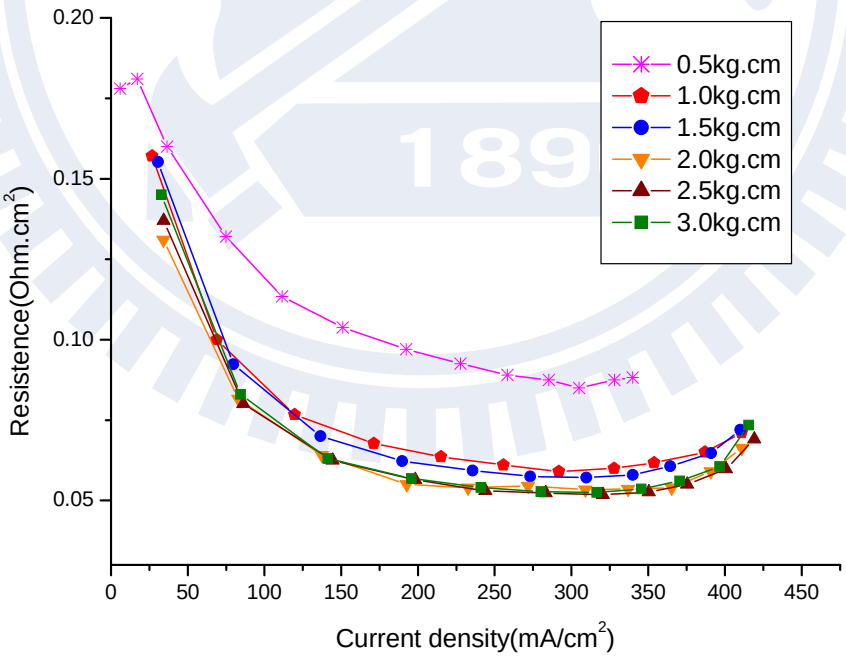

Fig. 4.14 I-R Curves of Clamping Fore Effect on Single Cell

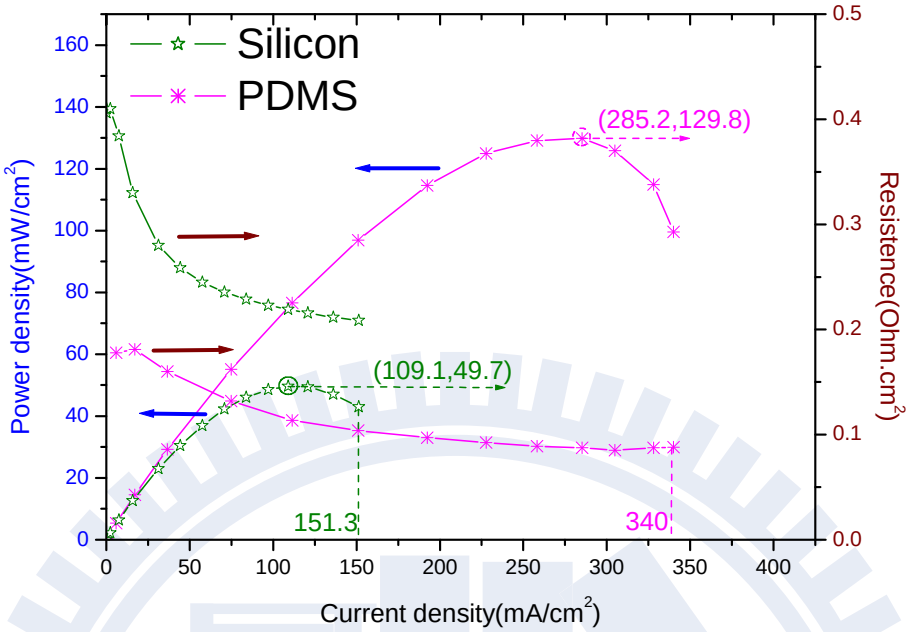

Fig. 4.15 Comparison of PDMS and Silicon Base

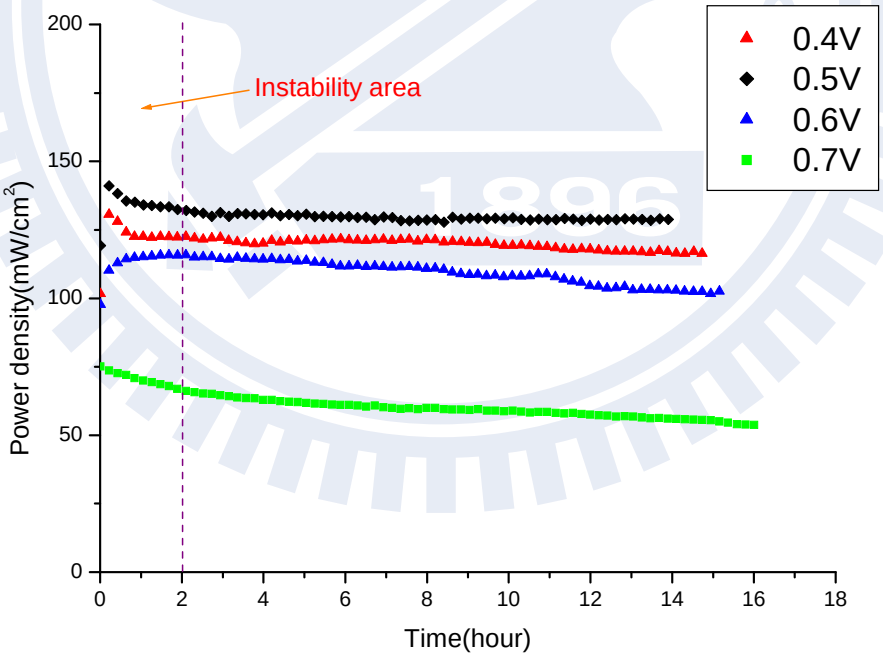

Fig. 4.16 Long Time Test of Single Micro PDMS PEMFC

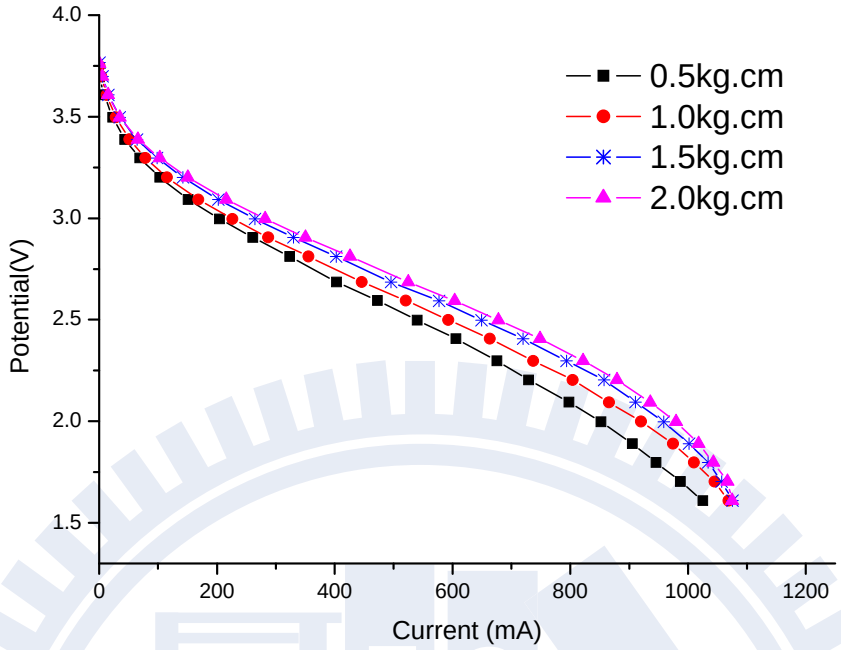

Fig. 4.17 I-V Curves of Clamping Force Effect on Micro Planar PEMFC Stack

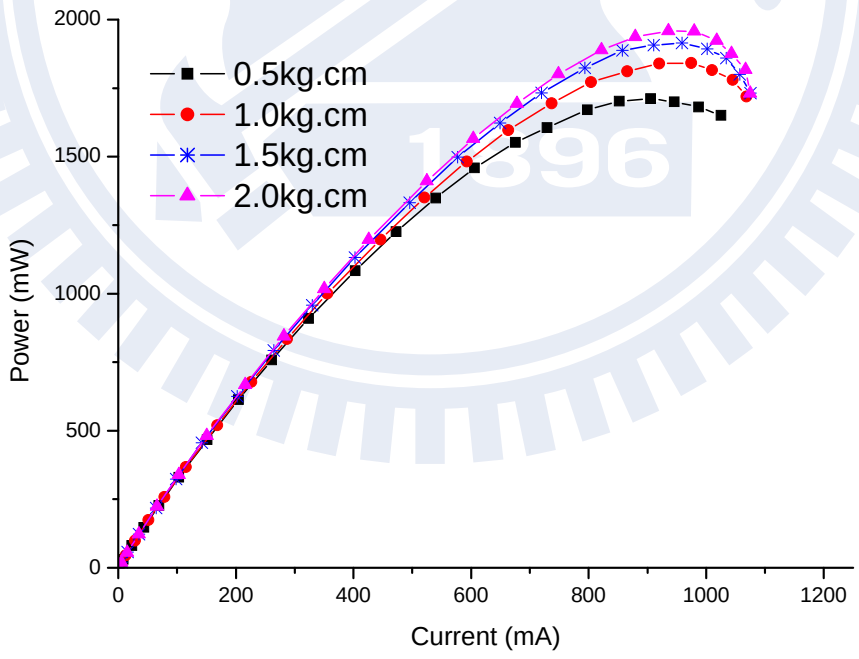

Fig. 4.18 I-P Curves of Clamping Force Effect on Micro Planar PEMFC Stack

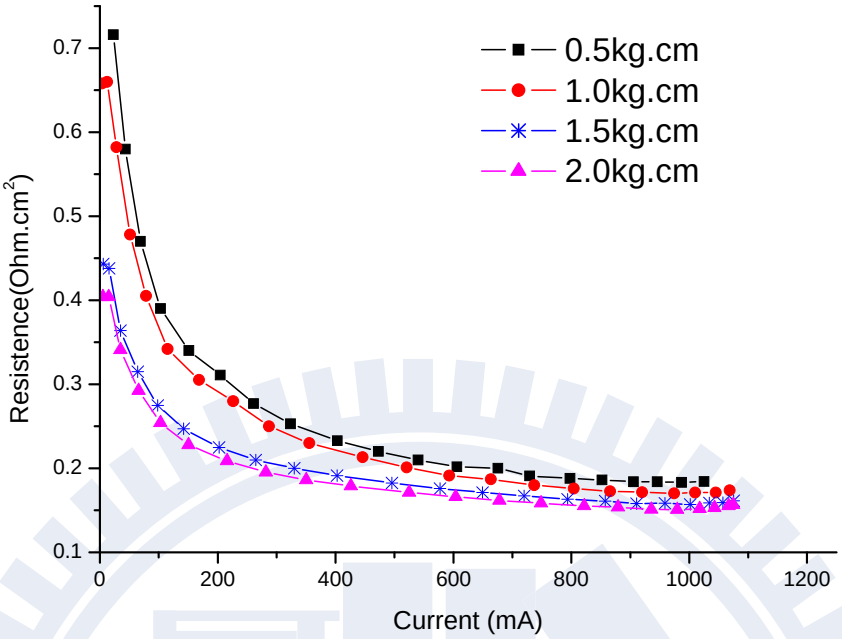

Fig. 4.19 I-R Curves of Clamping Force Effect on Micro Planar PEMFC Stack

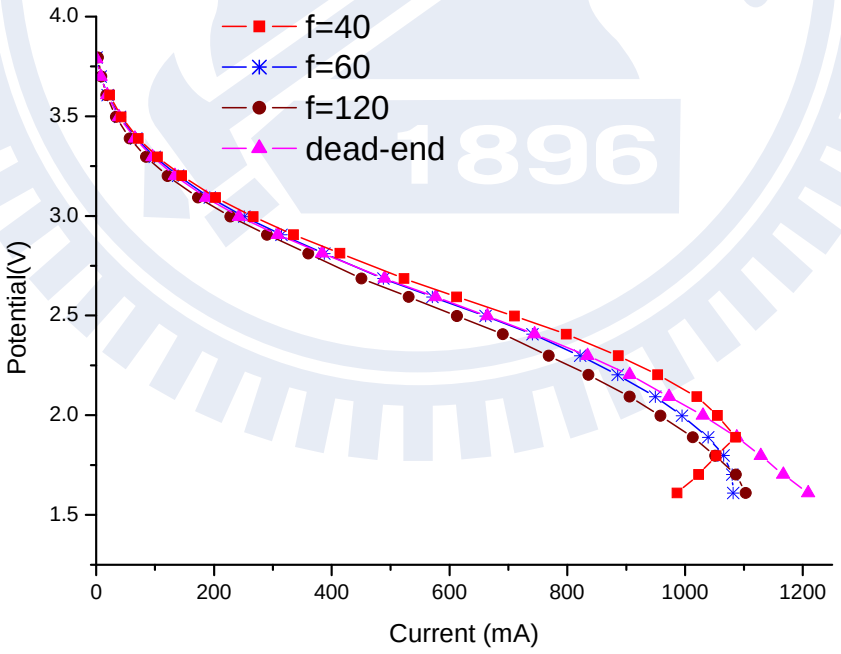

Fig. 4.20 I-V Curves of Different Fuel Supply Condition of Micro Planar PEMFC Stack

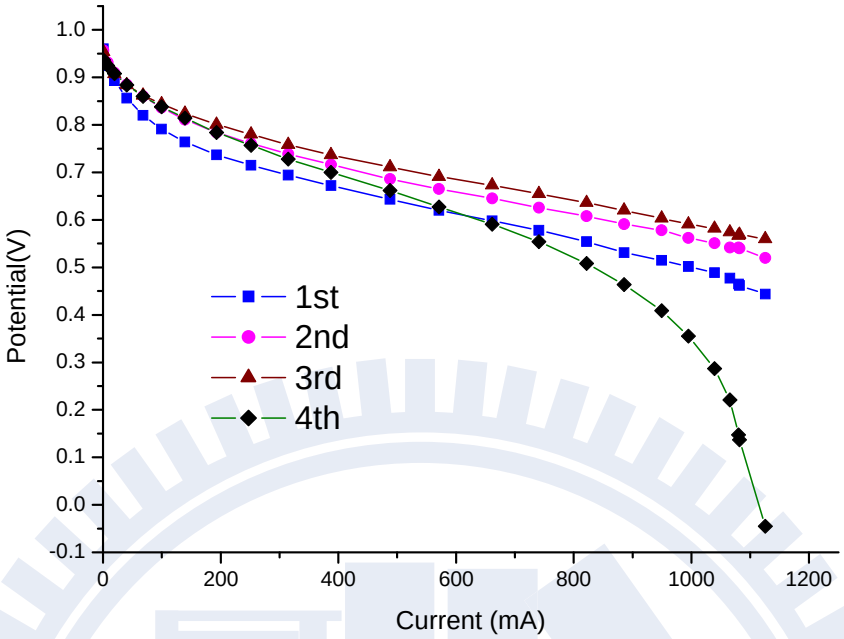

Fig. 4.21 I-V Curves of Each Cell under Fuel Flow Rate of 60sccm

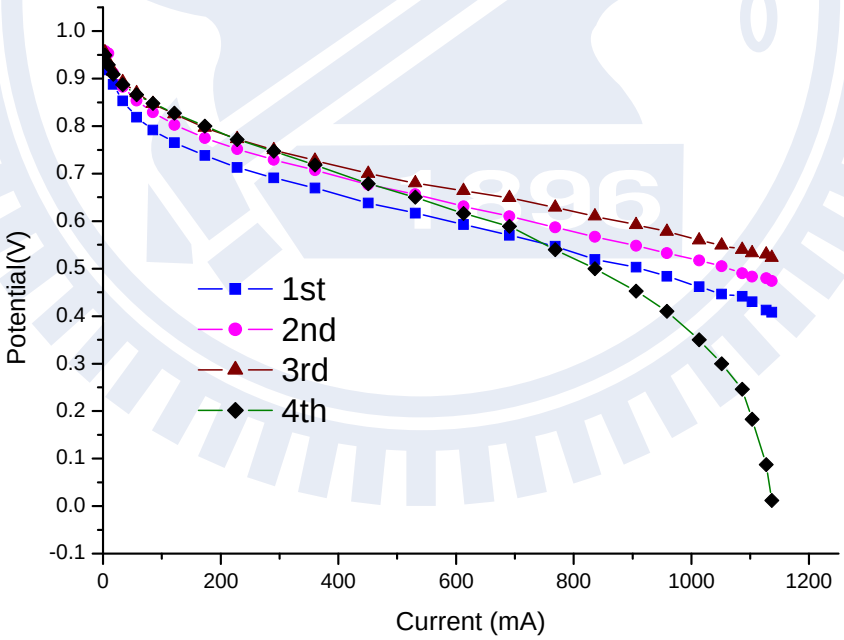

Fig. 4.22 I-V Curves of Each Cell under Fuel Flow Rate of 120sccm

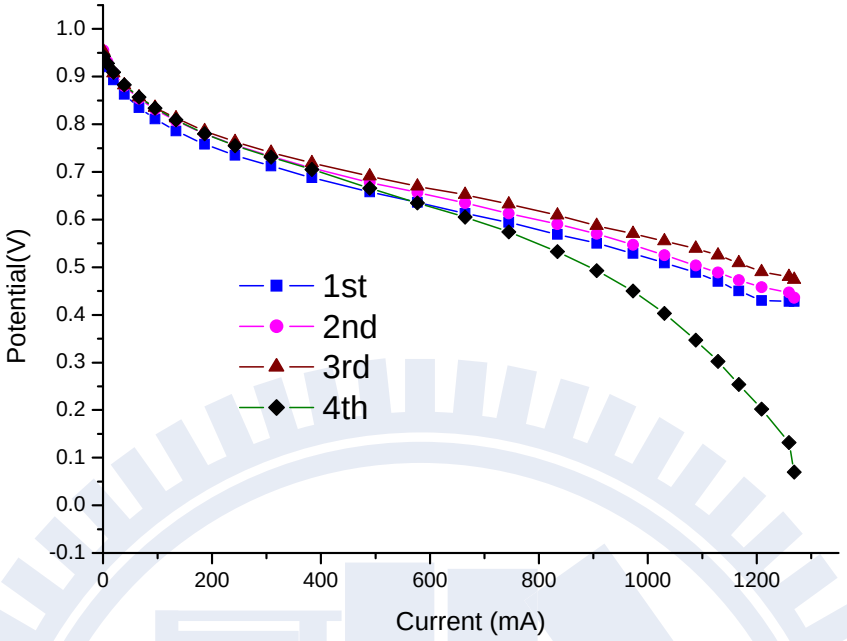

Fig. 4.23 I-V Curves of Each Cell under Dead-end Condition

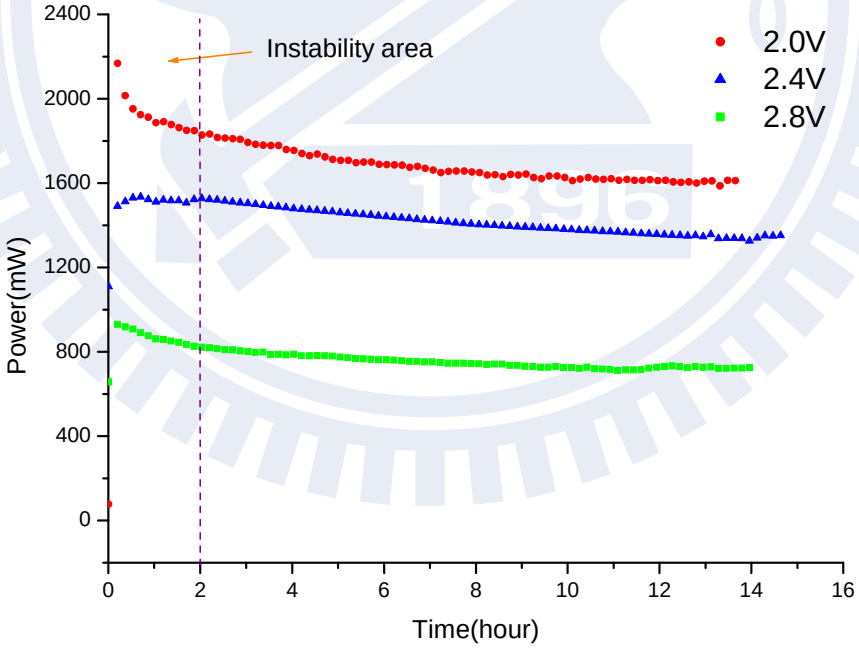

Fig. 4.24 Long time test of Planar Micro PDMS PEMFC Stack

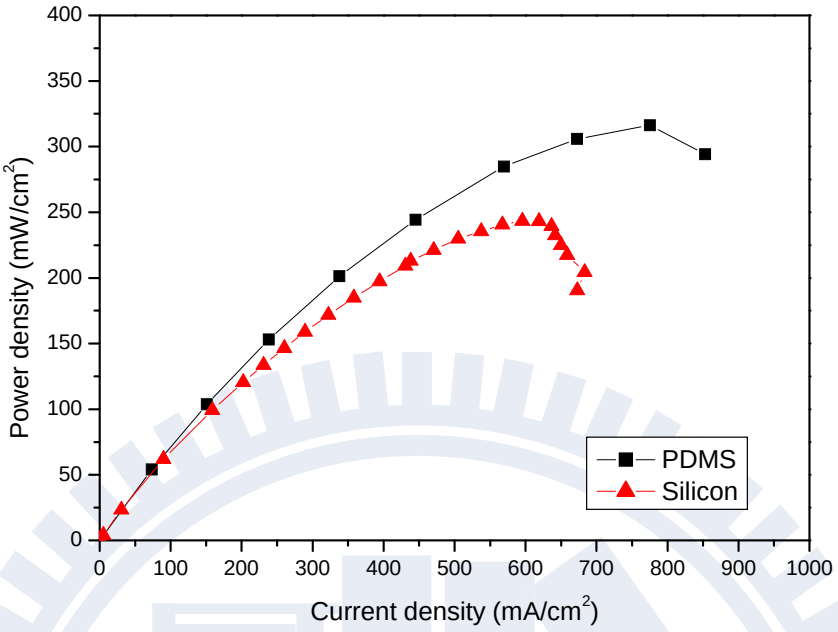

Fig. 4.25 Comparison of PDMS-Based and Silicon-Based PEMFC when using Oxygen

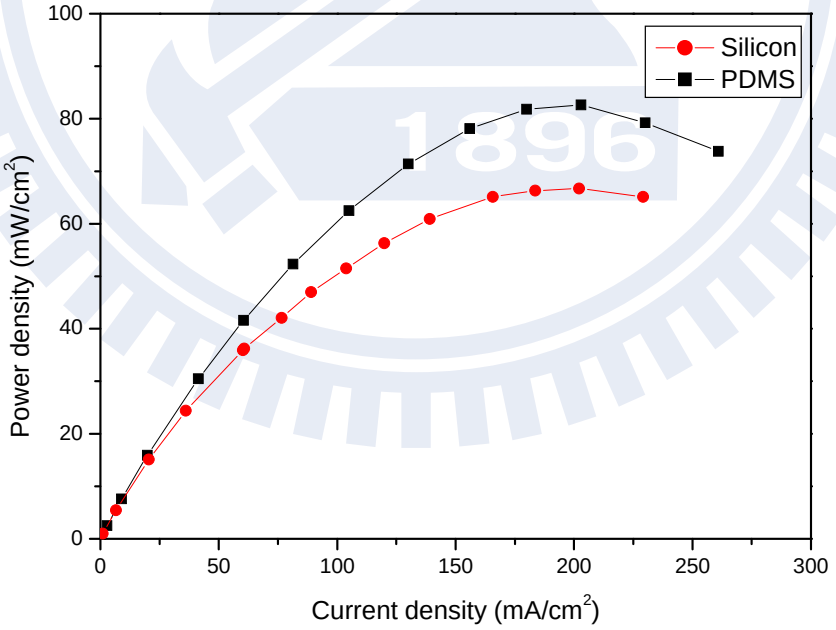

Fig. 4.26 Comparison of PDMS-Based and Silicon-Based PEMFCs when Air-breathing

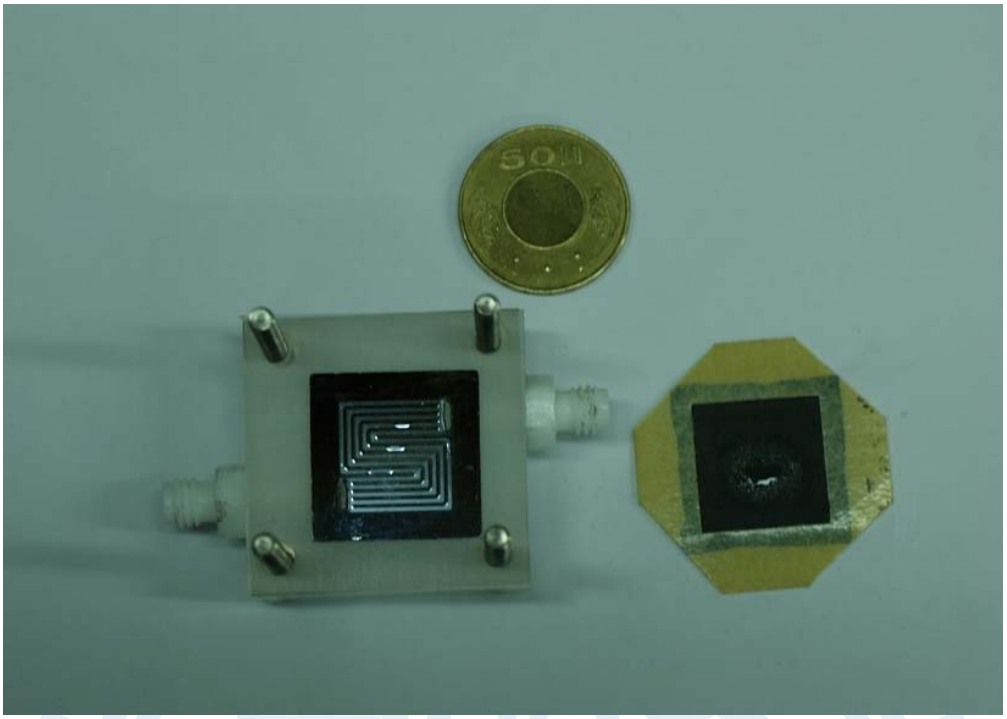

Fig. 4.27 Liquid Water on Silicon-based Flow Field Plate and GDL

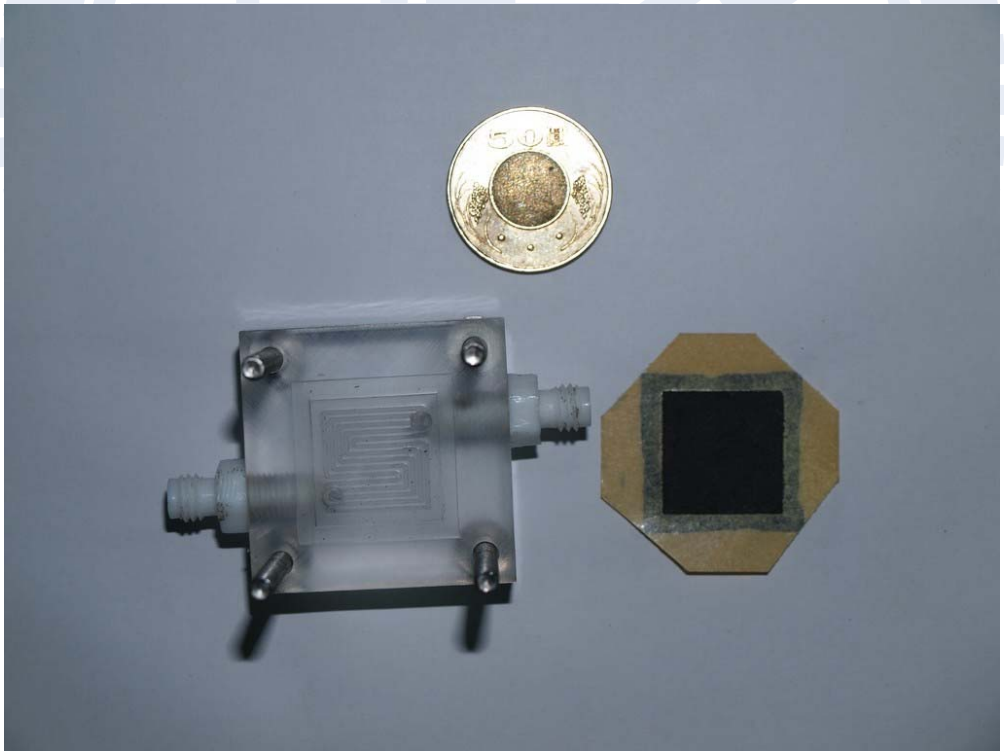

Fig. 4.28 No Water on PDMS-based Flow Field Plate and GDL

Chapter 5

Conclusions and Recommendations

5.1 Conclusions

This study is divided into three parts. Firstly, a series of performance experiments on a single micro PDMS PEMFC was carried out and demonstrated. The experimental parameters included current collector shape, convection type and clamping force, respectively. Secondly, a planar PEMFC stack was designed and assembled to test the performance. The experimental parameters consisted of clamping force and fuel supply condition. In addition, in order to see the durability of continuous usage, both the single cell and the stack were tested for 14 hours at a fixed operating voltage. Finally, a comparison between PDMS-based PEMFC and silicon-based one was made to see the feasibility of micro PEMFC, which was fabricated by using PDMS as the material of the flow field plate and used the new design that combined both the gasket and flow field on the same plate.

According to above experiment results, this study can obtain the following conclusions:

1. The performance of the air-breathing cell increases with an increase of the circle numbers from one to twenty-five on the current collector under the same current collector open ratio.
2. The performance trend of the forced convection cell is quite similar to that of air-breathing single cell at high current density region. The qualitative difference in performance among these shapes of current collectors is not affected by the convection way.

3. The forced convection cell is a better choice for long-time high current-density output; in contrast, the air-breathing cell is more suitable for lower current density output.
4. An appropriate clamping torque should be considered carefully to enhance the performance without damaging the GDL and narrowing down the fuel flow channels. In the present study, a torque of 2.5 Kgf • cm is recommended in the single air-breathing cell. And the PDMS-based PEMFC performed much better than the Silicon-based one under the same clamping torque of 0.5. Kgf • cm.
5. For the stack, the assembly force cannot be over a certain limit, because the performance will not be further improved but damages of the GDL and flow channels can be possibly caused.
6. The increase of flow rate is not a best way to improve the concentration loss in the air-breathing stack because of the limited air supply.
7. Owing to the temperature and the concentration loss effects, each cell in the same stack has different performance under the design (in series arrangement) in this work.
8. Both the single micro PDMS fuel cell and the cell stack can maintain a stable power output for a long time use up to 14 hours.
9. The PDMS-based one has a better performance with a 24% of peak power more than that of the silicon-based one under forced oxygen supply, and has a better performance with a 24.5% of peak power for the air-breathing.
10. PDMS is a better material than silicon for micro air-breathing fuel

cell because it is with less water flooding effects.

5.2 Recommendations

This thesis has some lacks on the experiment. Followings are the recommendations for the near future development of micro PEMFC:

1. Observing the air-breathing cell's temperature distribution in cathode in order to see the effect on water forming.
2. Measuring the flow rate at the outlet of fuel flow channel to see the ratio of fuel utilized.
3. Using the Taguchi method to evaluate which and how the parameters affect the cell performance.
4. Trying different stack or flow channel design to improve the performance of the cell stack.

Reference

[1] C.W. Cheng, “The Experimental Study on Micro PEMFC by Using MEMS Technology”, June 2009.

[2] J. Yu, P. Cheng, Z. Ma, B. Yi, ”Fabrication of miniature silicon wafer fuel cells with improved performance, Journal of Power Sources, 124, pp. 40-46, May 2003.

[3] J.P. Meyers, H.L. Maynard, “Design considerations for miniaturized PEM fuel cells”, Journal of Power Sources, 109, pp. 76-88, 2002.

[4] C.S. Spiegel, R. Agarwal, S. Bhansali, ”Comparison of microchannel dimensions for air-breathing polymer exchange membrane microfuel cells”, Journal of Power Sources, 182, pp. 603–608, 2008.

[5] J.Y. Kim, O.J. Kwon, S.M. Hwang, M.S. Kang, J.J. Kim, ”Development of a miniaturized polymer electrolyte membrane fuel cell with silicon separators”, Journal of Power Sources, 161, pp. 432–436, 2006.

[6] Z. Xiao, G. Yan, C. Feng, P.C.H. Chan, I.M. Hsing, “Integrated fuel cell micro power system by microfabrication technique”, Transducers '05, Digest of Technical Papers, Vols 1 and 2, pp. 1856-1859, 2005.

[7] S.S. Hsieh, J.K. Kuo, C.F. Hwang, H.H. Tsai**,** **“**A novel design and microfabrication for a micro PEMFC”, Microsystem Technologies, 10, pp. 121–126, 2004.

[8] S.S. Hsieh, C.F. Huang, J.K. Kuo, “SU-8 flow field plates for a micro PEMFC”, J Solid State Electrochem, 9, pp. 121–131, 2005.

[9] K. Shah, W.C. Shin, R.S. Besser, ” A PDMS micro proton exchange membrane fuel cell by conventional and non-conventional

microfabrication techniques", Sensors and Actuators B, 97, pp. 157–167, 2004.

[10] Y.A. Song, C. Batista, R. Sarpeshkar, J. Han, " Rapid fabrication of microfluidic polymer electrolyte membrane fuel cell in PDMS by surface patterning of perfluorinated ion-exchange resin", Journal of Power Sources, 183, pp. 674–677, 2008.

[11] C.P.B. Siu, M. Chiao, "A Microfabricated PDMS Microbial Fuel Cell", Journal of Microelectromechanical System, vol. 17, no. 6, 2008.

[12] S.J. Lee, A. C. Chien, S.W. Cha, R. O'Hayre, Y.I. Park, Y. Saito, F.B. Prinz, " Design and fabrication of a micro fuel cell array with "flip-flop" interconnection", Journal of Power Sources, 112, pp. 410–418, 2002.

[13] T. Yang, P. Shi, "A preliminary study of a six-cell stack with dead-end anode and open-slits cathode", International Journal of Hydrogen Energy, 33, pp. 2795 – 2801, 2008.

[14] C.Y. Chen, W.H. La, B.J. Weng, H.J. Chuang, C.Y. Hsieh, C.C. Kung, " Planar array stack design aided by rapid prototyping in development of air-breathing PEMFC", Journal of Power Sources, 179, pp. 147–154, 2008.

[15] S.H. Kim, H.Y. Cha, C.M. Miesse, J.H. Jang, Y.S. Oh, S.W. Cha, "Air-breathing miniature planar stack using the flexible printed circuit board as a current collector", International Journal of Hydrogen Energy, 34, pp. 459-466, 2009.

[16] S.W. Cha, R. O'Hayre, Y. Saito, F. B. Prinz, "The scaling behavior of flow patterns: a model investigation", Journal of Power Sources,

134, pp. 57-71, 2004.

[17] M. Noponen, T. Mennola, M. Mikkola, T. Hottinen, P. Lund, “Measurement of current distribution in a free-breathing PEMFC”, Journal of Power Sources, 106, pp. 304–312, 2002.

[18] H. Sun, G. Zhang, L.J. Guo, S. Dehua, H. Liu, “Effects of humidification temperatures on local current characteristics in a PEM fuel cell”, Journal of Power Sources, 168, pp. 400–407, 2007.

[19] W.K. Lee, C.H. Ho, J.W. Van Zee, M. Murthy, “The effects of compression and gas diffusion layers on the performance of a PEM fuel cell”, Journal of Power Sources, 84, pp. 45–51, 1999.

[20] N. Fekrazad, T.L. Bergman, “Effect of Nonuniform Stack Compression on Proton Exchange Membrane Fuel Cell Temperature Distributions”, Journal of Heat Transfer, Vol. 130 / 122002-7, 2008.

[21] Y. Lu, R.G. Reddy, “Investigation of micro-PEM fuel cell using experimental and modeling methods”, Electrochimica Acta, 54, pp. 3952 – 3959, 2009.

[22] J.H. Lin, W.H. Chen, Y.J. Su, T.H. Ko, “Effect of gas diffusion layer compression on the performance in a proton exchange membrane fuel cell “, Fuel , 87, pp. 2420 – 2424, 2008.

[23] W.R. Chang, J.J. Hwang, F.B. Weng, S.H. Chan, “Effect of clamping pressure on the performance of a PEM fuel cell”, Journal of Power Sources, 166, pp. 149 – 154, 2007.

[24] Y. Zhou, G. Lin, A.J. Shih, S.J. Hu, “Assembly pressure and membrane swelling in PEM fuel cells”, Journal of Power Sources,

192, pp. 544 – 551, 2009.

[25] C.Y. Wen, Y.S. Lin, C.H. Lu, “Experimental study of clamping effects on the performances of a single proton exchange membrane fuel cell and a 10-cell stack”, Journal of Power Sources, 192, pp. 475 – 485, 2009.

[26] J. Larminie, A. Dicks, “Fuel Cell Systems Explained”.

APPENDIX A

PEMFC

The measuring uncertainty of fuel cell voltage and current are (U_V,U_I)

The minimum scale of measuring voltage in the apparatus=1mV

The voltage of the largest power V=533mV

The measuring uncertainty of voltage

$$U_v = \pm\frac{0.5}{533} = \pm 0.001$$

The minimum scale of measuring current in the apparatus=0.1mA

The current of the largest power I=2204.4mA

The measuring uncertainty of current

$$U_I = \pm\frac{0.05}{2204.4} = \pm 0.0002$$

The measuring uncertainty of fuel cell power (U_P)

$$P = I \times V$$

$$U_P = \sqrt{(U_V)^2 + (U_I)^2}$$

U_p=±0.001

Micro PEMFC

The measuring uncertainty of fuel cell voltage and current are (U_V,U_I)

The minimum scale of measuring voltage in the apparatus=1mV

The voltage of the largest power V=409mV

The measuring uncertainty of voltage

$$U_v = \pm\frac{0.5}{409} = \pm 0.001$$

The minimum scale of measuring current in the apparatus=0.1mA

The current of the largest power I=348.0mA

The measuring uncertainty of current

$$U_I = \pm\frac{0.05}{348.0} = \pm 0.0001$$

The measuring uncertainty of fuel cell power (U_P)

$$P=I\times V$$

$$U_P = \sqrt{(U_V)^2 + (U_I)^2}$$

$$U_p=\pm 0.001$$